Title
Instability of catenary-type flexible risers conveying fluid in subsea environments

Journal
Ocean Engineering, 173

ISSN
0029-8018

Authors
Kim, Hyung-Taek
O'Reilly, Oliver M

Publication Date
2019-02-01

DOI
10.1016/j.oceaneng.2018.12.042

Peer reviewed

Instability of Catenary-Type Flexible Risers Conveying Fluid in Subsea Environments

Hyung-Taek Kim[a], Oliver M. O'Reilly[a,*]

[a]*Department of Mechanical Engineering, University of California at Berkeley, Berkeley CA 94720, USA*

Abstract

As water depths for oil and gas exploration and extraction increase, structures such as flexible risers, mooring lines, and umbilical cables are increasingly being used for subsea environments. Compared to conventional fixed-type structures and vertical risers, the dynamics of flexible risers is significantly more complex. In particular, the flexible structures may be prone to dynamic instabilities. The goal of the present paper is to provide a comprehensive study of the dynamics, stability, and vibration of flexible risers. We use Kirchhoff's theory of an extensible, flexible rod that resists torsion to develop a set of nonlinear equations for the dynamics of risers. The resulting model incorporates drag and the effects of the fluid being transported internally. Using a nonlinear stability criterion, our analyses show the nonlinear stability of a simple catenary-type riser modeled either as an inextensible or extensible string. For the more advanced rod models, we use a linear stability analysis to show how the internal fluid being conveyed can destabilize certain static configurations.

Keywords: flexible riser, Kirchhoff's rod theory, stability, top tension,

1. Introduction

As water depths for oil and gas exploration and extraction increase, structures such as flexible risers, mooring lines, and umbilical cables are increasingly being used for subsea environments. Compared to conventional fixed-type structures and vertical risers, the dynamics of flexible risers is significantly more complex. In particular, the flexible structures may be prone to dynamic instabilities. Furthermore, the massive weight of these flexible structures is often an issue in the design stage for both the suspended structures in the water as well as the surface structures that are used to deploy them. For economic and environmental reasons, studies of the dynamics of these massive flexible structures are worthy endeavors. The purpose of the present paper is to present the most comprehensive treatment of the dynamics of these structures to date.

*Corresponding author, Tel.: +1 510 642 0877, oreilly@berkeley.edu

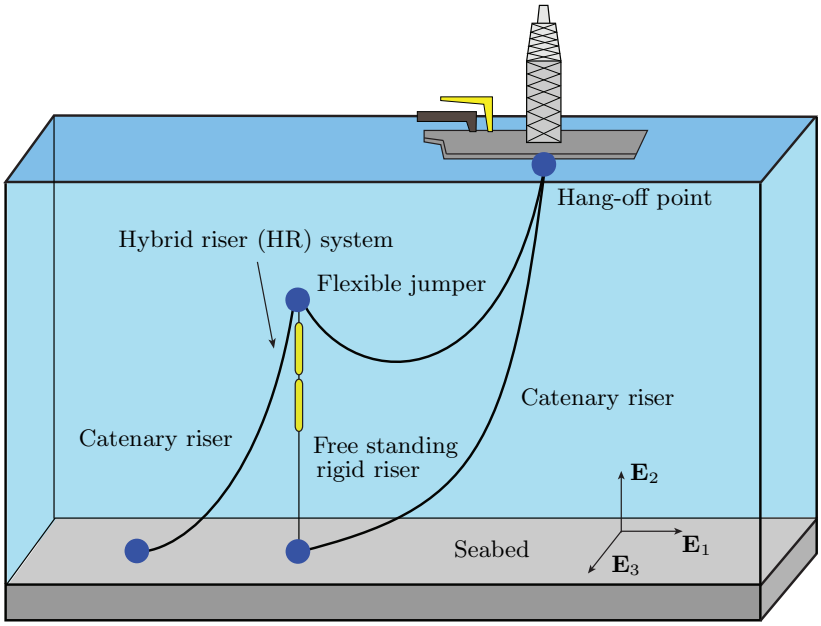

Fig. 1. Steel catenary riser (SCR) and a hybrid riser (HR) system used in marine environments for oil and gas development process. The SCR can be used either in a standalone manner to connect the surface vessel to the seabed or as a lower or upper part of a HR system.

Flexible risers, one of the most popular types of flexible structure and widely used for oil and gas exploration and transfer processes of hydrocarbons, particularly in deep or ultra-deep water conditions, fall into two categories: catenary-type risers that are used to provide a direct connection from the seabed to a surface vessel and lazy-type or steep wave-type risers equipped with a buoyancy module in the middle (Bai and Bai (2005)). Catenary-type risers that have been used in a various ways shown in Fig. 1 can be divided into two groups: those that couple directly with both the seabed and the surface vessel and those that serve as the lower part of a hybrid riser (HR) system or a buoyancy supported riser (BSR) that is decoupled from the motion of the surface vessel. Recently, even the upper part of the hybrid riser for which the flexible jumper is mainly used has been replaced with a catenary-type riser structure known as a steel catenary jumper (SCJ), as the conventional flexible jumper reaches the limit under more severe environmental conditions (cf. Rombado et al. (2012)).

Inspired by the pioneering works of Garrett (1982) and Nordgren (1974) a significant amount of work has been performed on the static and dynamic analyses of flexible structures in ocean environments (cf. the reviews by Ertas and Kozik (1987) and Patel and Seyed (1995)). We mention in particular the extensive studies on the simple catenary-type riser considering large deflection due to large gravity and other hydrodynamic forces by Chucheepsakul et al. (2003) and Chatjigeorgiou (2008). These works have recently been extended to include static and dynamic analyses for various types of risers equipped with a buoyancy module. In particular, parametric studies to investigate the effect of

design parameters such as external current and internal fluid speed on the equilibrium configurations of risers have been performed for a steep wave-type riser by Santillan et al. (2010), and a lazy wave-type riser by Wang et al. (2014) and Ruan et al. (2014).

Most of the works we have discussed above, i.e., static and dynamic analysis of flexible risers, are based on numerical methods including the finite element method (e.g., Garrett (1982), Nordgren (1974), Chucheepsakul et al. (2003), Chatjigeorgiou (2008), and Wang et al. (2014)) or a finite difference method (e.g., Santillan et al. (2010)) and are all well within the current capabilities of commercial riser design tools such as Orcaflex or Flexcom. Stability analysis, however, is not directly performed by these commercial packages. Furthermore, as highlighted in this paper, it is important to examine the stability of the riser when the internal fluid is being transported by the riser to and from the seabed to the surface vessel.

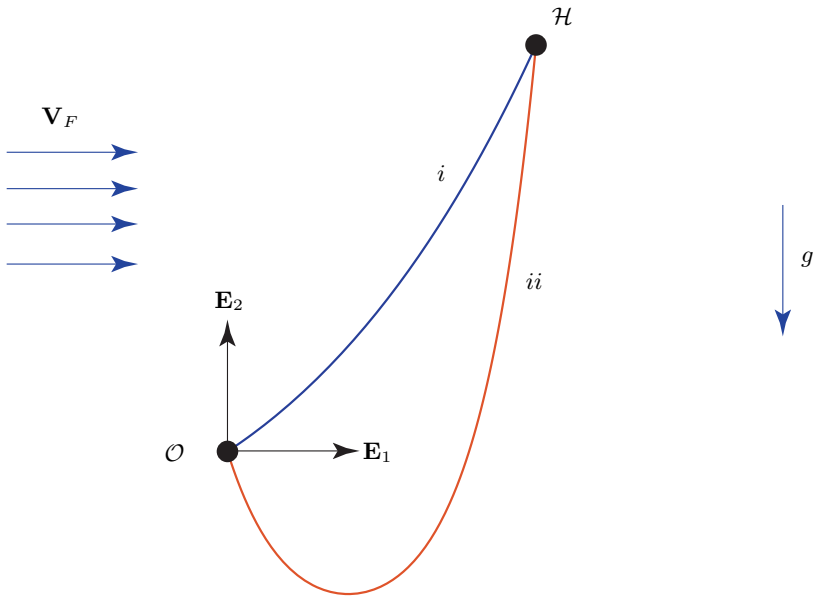

Fig. 2. A pair of static riser configurations that have the same magnitude of tension at the hang-off point $\mathcal{H}$. Our results show that for a variety of models, the shorter riser, which is labeled i, is stable while the longer riser, which is labeled ii, only becomes unstable in a flutter-type instability provided the effects of fluid transport in the riser are included in the model.

Given the enormous weight of the long structure in the ocean environment and the fluid-structure interaction between the riser, surrounding water, and the fluid that the riser is transporting, much of the analysis of the dynamics (vibrations) of these structures must be performed numerically (see, for example, Santillan et al. (2010), Chatjigeorgiou (2010), and Neto and Martins (2013)). However, some benchmark problems that simplify the effects of the fluid are often studied. For instance, Chucheepsakul and Wang (1997) examined the static configuration of a neutrally buoyant cable suspended between two points where the current is modeled as a constant load. They found that for the same magnitude of the tension force at one of the ends (a so-called "top tension"), two

configurations (of different lengths) are possible. Additionally, the authors found a critical top tension below which no equilibrium configurations of the cable were possible (cf. Fig. 2 for two representative configurations). In later works (Chucheepsakul and Monprapussorn (2001), Athisakul et al. (2014)), bending and extensibility were incorporated into their models and a stability criterion was established. The researchers argued that for a pair of static configurations with the same top tension, the one with the shorter (longer) length is stable (unstable). Their stability criterion is based on Euler's method of adjacent equilibria.[1]

In this paper, we complement Chucheepsakul et al.'s works by establishing a nonlinear stability criterion for the simplest models of risers. We supplement this criterion with a linear stability analysis based on a modal analysis that we then apply to more realistic models of risers. Using a variational principle, we find that the static configurations of the riser predicted by the simplest models are nonlinearly stable. However, when a more realistic rod model incorporating the effects of the internal fluid flow in the riser is analyzed and a linear stability analysis is performed, then we find that some of the static configurations can be destabilized. As summarized in Fig. 2, of the two configurations with the same top tension, both are stable if the effects of fluid transport are ignored. However, when this effect is included, then the configuration with the longer deformed length will destabilize while the one with the shorter deformed length will remain stable.

The instability responsible for destabilizing the longer configuration can be classified as an out-of-plane flutter-type instability and is similar to the instabilities in vertical risers transporting fluid that are discussed by Païdoussis (2014) and Monprapussorn et al. (2006), among others.[2] For the vertical riser, a critical speed of fluid flow is present, however for the catenary-type risers we consider, the flutter instability manifests for certain static configurations when the speed of the internal fluid flow is non-zero. In addition, the instability involves two pairs of complex conjugate eigenvalues crossing the imaginary axis and can be considered as a double Hopf bifurcation.

An outline of the paper is as follows. To present a comprehensive treatment of the dynamics of the stability of flexible catenary-type risers, we model the riser as a flexible, extensible elastic rod which is capable of twisting. We model the rod using Kirchhoff's theory of an elastic rod and incorporate fluid-structure interactions using drag and added-mass effects, among others. The resulting two-point boundary value problem for static configurations of the riser is solved using numerical methods for a wide variety of cases. In particular, we validate our code by comparing the results to numerous published works on both vertical and catenary risers. We also use a nonlinear stability criterion to elucidate the stability of neutrally buoyant cables under constant forces regardless of their top tensions and then apply it to more realistic riser models. The equations governing the vibrations of the riser and their associated mode shapes are also discussed. Parametric studies are then carried out to quantitatively examine the effect of external current and internal fluid on the dynamics of the riser and to show how instabilities can be present.

[1] For details on, and additional references to, this stability criterion, the reader is referred to Atanackovic (1997).

[2] For additional background on instabilities induced by fluids that a pipe is conveying, we refer the reader to the recent review Doaré (2019) as well as the seminal work Païdoussis (2014).

2. Modeling a flexible riser

Flexible risers are modeled using a variety of string and rod theories in the literature. These one-dimensional continua are subject to a variety of forces ranging from gravity and buoyancy forces to drag and added mass effects. The simplest model in this hierarchy of models is an inextensible string, the next is an extensible string, followed by a planar rod theory known as the elastica. The highest member of this hierarchy to date is a rod theory that accommodates bending, torsion, and, in some papers, extension. This is known as Kirchhoff's rod theory and relevant background on this rod theory can be found in a variety of textbooks including Antman (2005), Love (1927), and O'Reilly (2017). The governing equations for a riser that are provided by Kirchhoff's rod theory reduce to those for an elastica and a string once certain effects are ignored. We shall exploit this fact later in this paper.

2.1. Kinematics and assumptions

The centerline of the riser is described by a smooth curve which is known as a material curve. In its reference state the arc-length parameter of the curve is defined using a coordinate ξ. The position point on the material curve in the deformed state is defined by the position vector $\mathbf{R}$. The position vector $\mathbf{R}$ can be described using a Cartesian coordinate system:

$$\mathbf{R}\left(\xi,t\right)=X\left(\xi,t\right)\mathbf{E}_1+Y\left(\xi,t\right)\mathbf{E}_2+Z\left(\xi,t\right)\mathbf{E}_3. \tag{2.1}$$

The arc-length of the material curve in its present configuration is defined by the coordinate S. The partial derivatives of $\mathbf{R}$ with respect to ξ and S are related by the stretch μ:

$$\frac{\partial S}{\partial \xi}=\mu. \tag{2.2}$$

That is,

$$\mathbf{R}'\left(\xi,t\right)=\frac{\partial \mathbf{R}}{\partial \xi}=\mu\frac{\partial \mathbf{R}}{\partial S}, \tag{2.3}$$

where the prime $'$ denotes the partial derivative with respect to ξ. The vector $\frac{\partial \mathbf{R}}{\partial S}$ is the unit tangent vector to the material curve in its present configuration.

At each point of the material curve a set of unit vectors are defined: $\mathbf{d}_\alpha=\mathbf{d}_\alpha(\xi,t)$ where $\alpha=1,2$. For the rod theory of interest, this pair of vectors along with the unit tangent vector form a right-handed orthonormal triad: $\left\{\mathbf{d}_1,\mathbf{d}_2,\mathbf{d}_3=\frac{\partial \mathbf{R}}{\partial S}\right\}$. We also assume that the centerline of the rod in the reference configuration is straight and aligned with $\mathbf{E}_3$. We can thus define an associated set of vectors $\{\mathbf{D}_1=\mathbf{E}_1,\mathbf{D}_2=\mathbf{E}_2,\mathbf{D}_3=\mathbf{E}_3\}$ at each material point of the material curve in the reference configuration and a rotation tensor $\mathbf{P}$ which transforms $\mathbf{D}_i$ to $\mathbf{d}_i$: $\mathbf{d}_i=\mathbf{P}\mathbf{D}_i$.

Because $\mathbf{P}$ is a rotation, the spatial and time derivatives of the director basis have the representations

$$\frac{\partial \mathbf{d}_i}{\partial \xi}=\mathbf{P}\boldsymbol{\nu}\times\mathbf{d}_i,\qquad \frac{\partial \mathbf{d}_i}{\partial t}=\boldsymbol{\omega}\times\mathbf{d}_i,\qquad i=1,2,3. \tag{2.4}$$

Here, the strain vector $\mathbf{P}\boldsymbol{\nu} = \sum_{i=1}^{3} \nu_i \mathbf{d}_i$ captures the bending strains ν_1 and ν_2 and torsional strain ν_3 while $\boldsymbol{\omega}$ is the angular velocity vector:

$$\begin{aligned} \boldsymbol{\nu}(\xi,t) &= \nu_1(\xi,t)\,\mathbf{D}_1 + \nu_2(\xi,t)\,\mathbf{D}_2 + \nu_3(\xi,t)\,\mathbf{D}_3, \\ \boldsymbol{\omega}(\xi,t) &= \omega_1(\xi,t)\,\mathbf{d}_1 + \omega_2(\xi,t)\,\mathbf{d}_2 + \omega_3(\xi,t)\,\mathbf{d}_3. \end{aligned} \tag{2.5}$$

The vectors $\boldsymbol{\nu}$ and $\boldsymbol{\omega}$ satisfy a well-known compatibility condition $\frac{\partial \boldsymbol{\nu}}{\partial t} = \mathbf{P}^T \frac{\partial \boldsymbol{\omega}}{\partial \xi}$.

In the sequel we parameterize $\mathbf{P}$ using a 3-2-3 set of Euler angles.[3] The following identities can be established in a straightforward manner:

$$\begin{bmatrix} \nu_1 \\ \nu_2 \\ \nu_3 \end{bmatrix} = \mathsf{A} \begin{bmatrix} \alpha_1' \\ \alpha_2' \\ \alpha_3' \end{bmatrix}, \quad \begin{bmatrix} \omega_1 \\ \omega_2 \\ \omega_3 \end{bmatrix} = \mathsf{A} \begin{bmatrix} \dot{\alpha}_1 \\ \dot{\alpha}_2 \\ \dot{\alpha}_3 \end{bmatrix}, \tag{2.6}$$

where the dot denotes the derivative of a function of ξ and t with respect to t keeping ξ fixed, and

$$\begin{aligned} \mathsf{A} &= \begin{bmatrix} -\sin(\alpha_2)\cos(\alpha_3) & \sin(\alpha_3) & 0 \\ \sin(\alpha_2)\sin(\alpha_3) & \cos(\alpha_3) & 0 \\ \cos(\alpha_2) & 0 & 1 \end{bmatrix}, \\ \mathsf{A}^{-1} &= \begin{bmatrix} -\operatorname{cosec}(\alpha_2)\cos(\alpha_3) & \operatorname{cosec}(\alpha_2)\sin(\alpha_3) & 0 \\ \sin(\alpha_3) & \cos(\alpha_3) & 0 \\ \cot(\alpha_2)\cos(\alpha_3) & -\cot(\alpha_2)\sin(\alpha_3) & 1 \end{bmatrix}. \end{aligned} \tag{2.7}$$

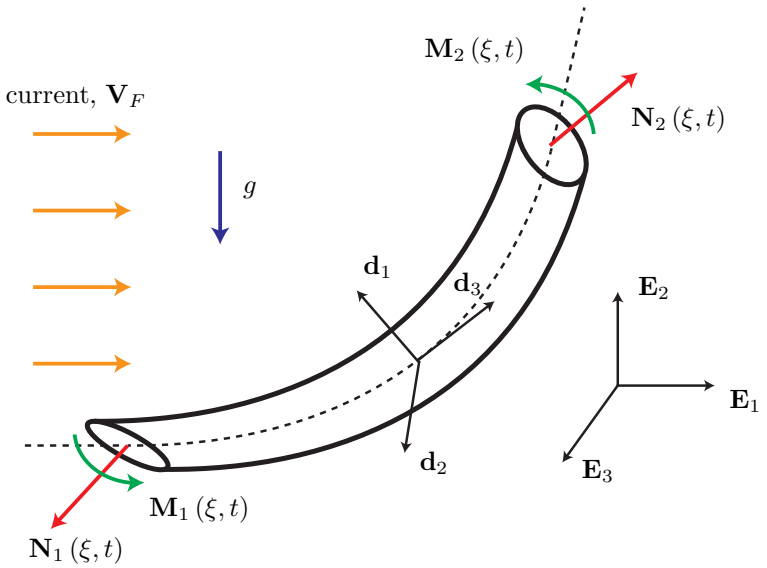

Fig. 3. Free-body diagram of an infinitesimal element of a rod that is used to model a flexible riser. The present configuration of the rod is described with the help of a local director basis $\mathbf{d}_i$ defined at each cross section. The vectors $\mathbf{N}$ and $\mathbf{M}$ represent the contact force and contact moment, respectively.

[3] This is the set of Euler angles used in Love (1927). For further details on this choice, see (O'Reilly, 2017, Section 5.3.1).

2.2. Constitutive relations

We assume that the reference configuration of the riser can be modeled as a straight rod with a uniform circular cross section. The mass density per unit length, cross sectional area, and areal moments of inertia of the rod in its reference state are denoted by $\rho_0 A$, A, I_1, and I_2, respectively. Assuming that the riser is composed of a linearly elastic material, the following classic strain energy function ψ can be prescribed:

$$2\rho_0 A\psi = EA\left(\mu-1\right)^2 + EI_1\nu_1^2 + EI_2\nu_2^2 + \mathcal{D}\nu_3^2, \tag{2.8}$$

where EA is the axial stiffness, $\mathcal{D}$ is the torsional stiffness, and EI_1 and EI_2 are bending stiffnesses. We shall assume that the bending stiffnesses are identical, i.e., the rod is isotropic: $(EI_1 = EI_2 = EI)$. It is convenient to express the contact force vector $\mathbf{N}$ and contact moment vector $\mathbf{M}$ in terms of the director basis as follows:

$$\begin{aligned}\mathbf{N}\left(\xi,t\right) &= N_1\left(\xi,t\right)\mathbf{d}_1 + N_2\left(\xi,t\right)\mathbf{d}_2 + N_3\left(\xi,t\right)\mathbf{d}_3,\\ \mathbf{M}\left(\xi,t\right) &= M_1\left(\xi,t\right)\mathbf{d}_1 + M_2\left(\xi,t\right)\mathbf{d}_2 + M_3\left(\xi,t\right)\mathbf{d}_3.\end{aligned} \tag{2.9}$$

The constitutive equations relating the components of $\mathbf{N}$ and $\mathbf{M}$ to the strain components are

$$\begin{aligned}\mathbf{N} &= N_1\mathbf{d}_1 + N_2\mathbf{d}_2 + EA\left(\mu-1\right)\mathbf{d}_3,\\ \mathbf{M} &= EI\nu_1\mathbf{d}_1 + EI\nu_2\mathbf{d}_2 + \mathcal{D}\nu_3\mathbf{d}_3.\end{aligned} \tag{2.10}$$

For a derivation of these relations using the strain energy function (2.8), the reader is referred to (O'Reilly, 2017, Section 5.9). We note that N_1 and N_2 are constraint or reaction forces that ensure that the rod is unshearable. Solving for these forces is part of the boundary-value problem for the rod.

If the rod is inextensible $(\mu = 1)$, then the strain energy function (2.8) simplifies to

$$2\rho_0 A\psi = EI_1\nu_1^2 + EI_2\nu_2^2 + \mathcal{D}\nu_3^2. \tag{2.11}$$

The constitutive relations for $\mathbf{N}$ and $\mathbf{M}$ in this case are

$$\begin{aligned}\mathbf{N} &= N_1\mathbf{d}_1 + N_2\mathbf{d}_2 + N_3\mathbf{d}_3,\\ \mathbf{M} &= EI\nu_1\mathbf{d}_1 + EI\nu_2\mathbf{d}_2 + \mathcal{D}\nu_3\mathbf{d}_3.\end{aligned} \tag{2.12}$$

Observe that all of the components of $\mathbf{N}$ in this case are constraint forces which ensure that the deformation of rod has no shear and the centerline remains inextensible.

2.3. Equations of motion

A free-body diagram of the rod modeling the riser is shown in Fig. 3. We apply a balance of linear momentum and a balance of angular momentum to the rod to obtain the following pair of partial differential equations:

$$\begin{aligned}\mathbf{N}' &= \rho_0 A\ddot{\mathbf{R}} - \mathbf{F},\\ \mathbf{M}' &= \mathbf{N}\times\mathbf{R}' + \rho_0 I\left(\mathbf{d}_1\times\ddot{\mathbf{d}}_1 + \mathbf{d}_2\times\ddot{\mathbf{d}}_2\right).\end{aligned} \tag{2.13}$$

Table 1. The values of the parameters used for the three models in our numerical analyses.

Parameter	Symbol	Unit	Model 1[a]	Model 2[b]	Model 3[c]
density of sea water	ρ_f	kg/m^3	1025	1024	1025
density of internal fluid	ρ_i	kg/m^3	-	998	998
density of riser	ρ_o	kg/m^3	4039.8	2442.4	7850
outer diameter	D_o	m	0.023	0.2154	0.26
inner diameter	D_i	m	–	–	0.20
area of outer pipe	A_o	m^2	4.16×10^{-4}	3.64×10^{-2}	2.17×10^{-2}
area of inner pipe[*]	A_i	m^2	–	–	3.14×10^{-2}
horizontal offset	X_H	m	300	350	450
vertical offset	$Y_H = H$	m	500	350	900
bending stiffness	EI	Nm^2	8.26×10^3	6.57×10^3	3.02×10^7
axial stiffness	EA	N	2.50×10^8	–	4.49×10^9
added mass coeff.	C_a	-	1.0	1.0	1.0
normal drag coeff.	C_n	-	1.0	1.0	0.7
tangential drag coeff.	C_t	-	0.05	–	0.03
prespecified top tension	T_H	kN	25	–	$0-3$
uniform current velocity	V_F	m/s	1.0278	$0-2$	$0-3$
internal fluid speed	V_i	m/s			$0-100$
gravitational constant	g	m/s^2	9.81	9.81	9.81

[a] Chucheepsakul and Srinil (2002).
[b] Santillan et al. (2010).
[c] Athisakul et al. (2014).
[*] inner pipe through which the internal flow is being transported.

The resultant external force acting on the riser per unit length is denoted by $\mathbf{F}$. This force is decomposed into the forces due to gravity $\mathbf{F}_g$, buoyancy $\mathbf{F}_b$, internal fluid $\mathbf{F}_i$, drag from external current $\mathbf{F}_d$ and an added mass effect $\mathbf{F}_a$;

$$\mathbf{F} = \mathbf{F}_g + \mathbf{F}_b + \mathbf{F}_i + \mathbf{F}_d + \mathbf{F}_a, \tag{2.14}$$

where

$$\begin{aligned}
\mathbf{F}_g &= -\rho_0 A g\ \mathbf{E}_2, \\
\mathbf{F}_b &= \rho_f A_o g\ \mathbf{E}_2, \\
\mathbf{F}_i &= -\rho_i A_i \mathbf{a}_i, \\
\mathbf{F}_d &= 0.5\,\rho_f D_o \left(C_n \left\|\mathbf{v}_{r_n}\right\| \mathbf{v}_{r_n} + \pi C_t \left\|\mathbf{v}_{r_t}\right\| \mathbf{v}_{r_t}\right), \\
\mathbf{F}_a &= -\rho_f A_o C_a \ddot{\mathbf{R}}.
\end{aligned} \tag{2.15}$$

The prescriptions for the drag and added mass forces are obtained from the generalized Morison equation (Morison et al. (1950)). The constants appearing in Eqn. (2.3) are defined in Table 1. The velocity vector $\mathbf{v}_f$ of the external current, the relative velocity vector $\mathbf{v}_r$ of the external current, and the velocity vector $\mathbf{v} = \dot{\mathbf{R}}$ of a material point on the centerline of the rod are used to compute the following tangential $\mathbf{v}_{r_t}$ and normal

$\mathbf{v}_{r_n}$ velocity vectors:

$$\begin{aligned}
\mathbf{v}_r &= \mathbf{v}_f - \mathbf{v}, \\
\mathbf{v}_{r_t} = (\mathbf{v}_r \cdot \mathbf{d}_3)\,\mathbf{d}_3, &\qquad \mathbf{v}_{r_n} = \mathbf{v}_{r_{n_1}} + \mathbf{v}_{r_{n_2}}, \\
\mathbf{v}_{r_{n_1}} = ((\mathbf{v}_r - \mathbf{v}_{r_t}) \cdot \mathbf{d}_1)\,\mathbf{d}_1, &\qquad \mathbf{v}_{r_{n_2}} = ((\mathbf{v}_r - \mathbf{v}_{r_t}) \cdot \mathbf{d}_2)\,\mathbf{d}_2.
\end{aligned} \tag{2.16}$$

The vector $\mathbf{a}_i$ is the acceleration vector of the fluid being transported by the riser. To establish this expression, we assume that the fluid is being transported axially through the riser so that the material coordinate of the fluid ξ_f is changing at a constant rate: $V_i = \frac{\partial \xi_f}{\partial t}$ (Chatjigeorgiou (2010) and (Païdoussis, 2014, Section 4)). Taking the time derivative of the position vector $\mathbf{r}_i = \mathbf{r}_i(\xi_f, t)$ of a fluid particle moving through the riser and invoking the chain rule we find that

$$\begin{aligned}
\mathbf{a}_i &= \frac{\partial^2 \mathbf{R}}{\partial t^2} + 2V_i \frac{\partial^2 \mathbf{R}}{\partial t \partial \xi} + V_i^2 \frac{\partial^2 \mathbf{R}}{\partial \xi^2} \\
&= \ddot{\mathbf{R}} + 2V_i \frac{\partial}{\partial t}(\mu \mathbf{d}_3) + V_i^2 \frac{\partial}{\partial \xi}(\mu \mathbf{d}_3) \\
&= \ddot{\mathbf{R}} + 2V_i\left(\dot{\mu}\mathbf{d}_3 + \mu(\omega_2 \mathbf{d}_1 - \omega_1 \mathbf{d}_2)\right) + V_i^2\left(\mu' \mathbf{d}_3 + \mu(\nu_2 \mathbf{d}_1 - \nu_1 \mathbf{d}_2)\right),
\end{aligned} \tag{2.17}$$

where the dot and prime are partial derivatives with respect to time t and arc-length ξ, respectively.

Employing the dimensionless scalings discussed in Appendix A, a set of nonlinear governing equations can be constructed from (2.13):

$$\begin{aligned}
n_1' &= \{(1 + C_a + \beta)\,\ddot{\mathbf{r}} + (w - b)\,\mathbf{E}_2\} \cdot \mathbf{d}_1 + 2\sqrt{\beta} v_i \mu \Omega_2 + v_i^2 \mu \bar{\nu}_2 - f_{n1} + n_2 \bar{\nu}_3 - n_3 \bar{\nu}_2, \\
n_2' &= \{(1 + C_a + \beta)\,\ddot{\mathbf{r}} + (w - b)\,\mathbf{E}_2\} \cdot \mathbf{d}_2 - 2\sqrt{\beta} v_i \mu \Omega_1 + v_i^2 \mu \bar{\nu}_1 - f_{n2} + n_3 \bar{\nu}_1 - n_1 \bar{\nu}_3, \\
n_3' &= \{(1 + C_a + \beta)\,\ddot{\mathbf{r}} + (w - b)\,\mathbf{E}_2\} \cdot \mathbf{d}_3 + 2\sqrt{\beta} v_i \dot{\mu} + v_i^2 \mu' - f_t + n_1 \bar{\nu}_2 - n_2 \bar{\nu}_1, \\
\bar{\nu}_1' &= (1 - \gamma)\,\bar{\nu}_2 \bar{\nu}_3 + \mu n_2 + \eta\left(\dot{\Omega}_1 + \Omega_2 \Omega_3\right), \\
\bar{\nu}_2' &= (\gamma - 1)\,\bar{\nu}_3 \bar{\nu}_1 - \mu n_1 + \eta\left(\dot{\Omega}_2 - \Omega_3 \Omega_1\right), \\
\bar{\nu}_3' &= \frac{2}{\gamma}\eta \dot{\Omega}_3, \\
\begin{bmatrix} \alpha_1' \\ \alpha_2' \\ \alpha_3' \end{bmatrix} &= \mathsf{A}^{-1} \begin{bmatrix} \bar{\nu}_1 \\ \bar{\nu}_2 \\ \bar{\nu}_3 \end{bmatrix}, \\
\begin{bmatrix} \Omega_1 \\ \Omega_2 \\ \Omega_3 \end{bmatrix} &= \mathsf{A} \begin{bmatrix} \dot{\alpha}_1 \\ \dot{\alpha}_2 \\ \dot{\alpha}_3 \end{bmatrix}, \qquad \begin{bmatrix} \dot{\Omega}_1 \\ \dot{\Omega}_2 \\ \dot{\Omega}_3 \end{bmatrix} = \mathsf{A} \begin{bmatrix} \ddot{\alpha}_1 \\ \ddot{\alpha}_2 \\ \ddot{\alpha}_3 \end{bmatrix} + \dot{\mathsf{A}} \begin{bmatrix} \dot{\alpha}_1 \\ \dot{\alpha}_2 \\ \dot{\alpha}_3 \end{bmatrix}, \\
x' &= \mu(\mathbf{d}_3 \cdot \mathbf{E}_1), \\
y' &= \mu(\mathbf{d}_3 \cdot \mathbf{E}_2), \\
z' &= \mu(\mathbf{d}_3 \cdot \mathbf{E}_3),
\end{aligned} \tag{2.18}$$

where, for an extensible rod,

$$\mu = 1 + \eta n_3. \tag{2.19}$$

In (2.18) and (2.19), all of the variables and derivatives are dimensionless. Henceforth, the $'$ denotes partial derivative with respect to a dimensionless arc-length $s = \xi/H$ and the dot denotes partial derivative with respect to a dimensionless time $\tau = \frac{t}{H^2}\sqrt{\frac{EI}{\rho_0 A}}$. We can express the solution $\mathsf{X}(s,\tau)$ to the equations (2.18) and (2.19) for a rod in the following compact form:

$$\mathsf{X} = \begin{cases} [n_1, n_2, \mu, \bar{\nu}_1, \bar{\nu}_2, \bar{\nu}_3, \alpha_1, \alpha_2, \alpha_3, x, y, z]^T & \text{extensible rod} \\ [n_1, n_2, n_3, \bar{\nu}_1, \bar{\nu}_2, \bar{\nu}_3, \alpha_1, \alpha_2, \alpha_3, x, y, z]^T & \text{inextensible rod} \end{cases} \tag{2.20}$$

Here, n_i, $\bar{\nu}_i$, α_i, μ, x, y and z are solution variables representing respectively internal force, strain, Euler angles, stretch, and the Cartesian coordinates of every point along the length of the riser at each instant in time. The dimensionless variables β, w, b, f_t, f_{n_1}, f_{n_2}, μ, and η in (2.18) are defined in Appendix A.

2.4. Static equilibrium configurations

Equilibrium configurations of the riser correspond to static solutions $\mathsf{X}_s = \mathsf{X}_s(s)$ to the equations of motion. Of particular interest to us in this paper are solutions with pinned boundary conditions at the ends $\mathcal{O}$ and $\mathcal{H}$ of the riser. The point $\mathcal{H}$ is known as the hang-off point. These boundary conditions are applied as follows:

$$\begin{aligned} &\text{At } \mathcal{O}: x = 0, \quad y = 0, \quad z = 0, \quad \bar{\nu}_1 = 0, \quad \bar{\nu}_2 = 0, \quad \bar{\nu}_3 = 0, \\ &\text{At } \mathcal{H}: x = x_H, \quad y = y_H, \quad z = z_H, \quad \bar{\nu}_1 = 0, \quad \bar{\nu}_2 = 0, \quad \bar{\nu}_3 = 0. \end{aligned} \tag{2.21}$$

The solutions $\mathsf{X}_s = \mathsf{X}_s(s)$ satisfy the nonlinear equations

$$\mathsf{X}_s' = \mathsf{F}(\mathsf{X}_s), \tag{2.22}$$

where $\mathsf{F}(\mathsf{X}_s)$ is a nonlinear vector-valued function that can be computed readily from (2.18). In the interests of brevity, we do not write the lengthy expression for the components of $\mathsf{F}(\mathsf{X}_s)$ here. In order to compute the static equilibrium configurations for the static case, the boundary-value problem is solved directly using the MATLAB built-in function 'bvp4c' which is a finite difference code that implements the 3-stage Lobatto IIIa formula (Shampine et al. (2003)). The finite difference scheme is supplemented by a continuation method (Wasserstrom (1973)) that helps us examine how the static configuration evolves as the system parameters are varied. As discussed in Appendix B, we validated our method to compute the static configurations by comparing our results with published works.

2.5. Vibrations and linear stability analysis

To examine the stability of a static configuration, we consider small amplitude perturbations $\epsilon\mathsf{X}_d = \epsilon\mathsf{X}_d(s,\tau)$ to this configuration. Using a standard procedure (see, for example, Neukirch et al. (2012)), we substitute

$$\mathsf{X} = \mathsf{X}_s + \epsilon\mathsf{X}_d + O(\epsilon^2), \tag{2.23}$$

into the set of equations (2.18), assume second or higher order terms in ϵ are negligible, and obtain the following set of linear equations to $O(\epsilon)$:

$$\mathsf{X}_d' = \mathsf{D}_1\mathsf{X}_d + \mathsf{D}_2\ddot{\mathsf{X}}_d, \tag{2.24}$$

where the square matrices D_1 and D_2 are functions of s. We now seek harmonic solutions to (2.24):

$$\mathsf{X}_d(s,\tau) = \bar{\mathsf{X}}_d(s)\exp(\lambda\tau), \tag{2.25}$$

where λ is a dimensionless complex variable. Substituting (2.25) into (2.24), a system of linear equations for the amplitude $\bar{\mathsf{X}}_d$ and complex variables λ are obtained:

$$\mathsf{X}_d' = \mathsf{D}(s,\lambda)\bar{\mathsf{X}}_d. \tag{2.26}$$

With the help of the boundary conditions, we can compute the eigenvalues and corresponding eigenmodes of the static configuration of the riser from (2.26), where the eigenvalues are expressed as

$$\lambda_n = \mathrm{Re}(\lambda_n) + i\mathrm{Im}(\lambda_n) = \delta_n + i\omega_n. \tag{2.27}$$

Using classic results from linear stability (see, for example, Atanackovic (1997)), we can also determine the stability of the static configuration of the riser by verifying that the real part of every single λs is negative. If the real part of a single λ is positive, then the static configuration is deemed to be (linearly) unstable. As discussed in Appendix B, we validated our computational method for computing the linear vibrations of the riser by comparing our results with a variety of published works.

3. Stability of a catenary-type riser modeled as a heavy cable using a string theory

The Kirchhoff rod theory-based model for the riser reduces to that for a string if the bending and torsional stiffnesses and inertias are ignored. If the riser is modeled as a string, then the governing equations for planar motions are

$$\frac{\partial \mathbf{N}}{\partial S} = -\mathbf{F} + \rho_0 A\frac{\partial^2 \mathbf{R}}{\partial t^2}. \tag{3.1}$$

The contact force in the string is parallel to the tangent vector to the string: $\mathbf{N} = N\mathbf{e}_t$. Depending on whether or not the string is inextensible we have

$$\mathbf{N} = \begin{cases} N(\xi,t)\,\mathbf{e}_t \text{ when the string is inextensible: i.e., } \mu = 1, \\ \rho_0 A\frac{\partial \psi}{\partial \mu}\mathbf{e}_t \text{ when the string is elastic} \end{cases} \tag{3.2}$$

Here, N is a tension force that must be determined as part of the solution to the boundary-value problem and $\rho_0 A\psi = \Psi(\mu,\xi)$ is the strain energy function of the string per unit length of ξ. For linearly elastic strings,

$$\Psi(\mu,\xi) = \frac{EA}{2}(\mu-1)^2, \tag{3.3}$$

and so $\mathbf{N} = EA(\mu-1)\mathbf{e}_t$.

For planar solutions, two of the Euler angles, α_2 and α_3, are zero and the Z coordinate vanishes. In addition,

$$\mathbf{R} = X\mathbf{E}_1 + Y\mathbf{E}_2, \qquad \mathbf{e}_t = \frac{\partial X}{\partial S}\mathbf{E}_1 + \frac{\partial Y}{\partial S}\mathbf{E}_2 = \cos(\alpha_1)\mathbf{E}_1 + \sin(\alpha_1)\mathbf{E}_2. \tag{3.4}$$

The boundary conditions for a riser modeled using a string which has a length ℓ_0 in its reference configuration and is fixed at $\mathcal{O}$ and $\mathcal{H}$ are

$$\mathbf{R}\left(0,t\right)=\mathbf{R}_{\mathcal{O}}=\mathbf{0},\qquad \mathbf{R}\left(\ell_0,t\right)=\mathbf{R}_{\mathcal{H}}=X_H\mathbf{E}_1+Y_H\mathbf{E}_2. \tag{3.5}$$

The so-called top tension T_{Top} in the string is the tension N at $\mathcal{H}$:

$$T_{\text{Top}}=\mathbf{N}\left(\ell_0,t\right)\cdot\mathbf{e}_t\left(\ell_0,t\right),\qquad T_x=\mathbf{N}\left(\ell_0,t\right)\cdot\mathbf{E}_1,\qquad T_y=\mathbf{N}\left(\ell_0,t\right)\cdot\mathbf{E}_2, \tag{3.6}$$

where we have also defined the horizontal and vertical components of $\mathbf{N}$.

3.1. Nonlinear stability criteria

In several simple models for risers, $\mathbf{F}$ is assumed to be a constant force. The vertical component of the $\mathbf{F}$ consists of a gravitational force and a buoyancy force, and the horizontal component is assumed to model the effects of a current on the riser. For this case, the motion of the string that is modeling the riser conserves energy $\mathcal{E}$ and a very simple nonlinear criterion for the stability of a static configuration of the string can be established. The principal component of the criterion is to check that the string is everywhere in tension.

The stability criterion we employ assumes that the ends of the cable are fixed and the loading is conservative. The total energy of nearby configurations are compared to the energy of the static configuration under consideration. If the energy of the static configuration is smaller than the energy of any possible adjacent configurations, then the static configuration is defined to be stable. The energy in question has the following representations depending on whether the string is elastic or inextensible:

$$\mathcal{E}=\begin{cases}\int_0^{\ell_0}\left(\frac{\rho_0 A}{2}\frac{\partial\mathbf{R}}{\partial t}\cdot\frac{\partial\mathbf{R}}{\partial t}-\mathbf{F}\cdot\mathbf{R}\right)d\xi+\int_0^{\ell_0}\frac{\Lambda}{2}\left(\frac{\partial\mathbf{R}}{\partial\xi}\cdot\frac{\partial\mathbf{R}}{\partial\xi}-1\right)d\xi \text{ for an inextensible string}\\ \int_0^{\ell_0}\left(\frac{\rho_0 A}{2}\frac{\partial\mathbf{R}}{\partial t}\cdot\frac{\partial\mathbf{R}}{\partial t}+\rho_0 A\psi-\mathbf{F}\cdot\mathbf{R}\right)d\xi \text{ for an elastic string}\end{cases} \tag{3.7}$$

The function Λ is a Lagrange multiplier. The first variation of these functionals vanish for solutions to the equations of motion (3.1) provided Λ is identified as the tension in the string: $\Lambda=N=N\left(\xi,t\right)$. Positive-definiteness of $\mathcal{E}$ and therefore nonlinear stability of the static equilibrium configuration can be concluded if the following simple criterion is satisfied for an inextensible string

$$N>0\ \forall\xi\in\left[0,\ell_0\right], \tag{SC-1}$$

and, for an extensible string,

$$N=\rho_0 A\frac{\partial\psi}{\partial\mu}>0\text{ and }\rho_0 A\frac{\partial^2\psi}{\partial\mu^2}-\frac{\rho_0 A}{\mu}\frac{\partial\psi}{\partial\mu}>0\ \forall\xi\in\left[0,\ell_0\right]. \tag{SC-2}$$

The proofs of these two nonlinear stability criteria can be found in O'Reilly (1996) and, in the interests of brevity, we refer the reader to this work for details. We remark that the criteria SC-1 and SC-2 are far easier to verify than a linear stability criterion based on computing the eigenmodes and eigenvalues from a linear vibration analysis of a riser's configuration.

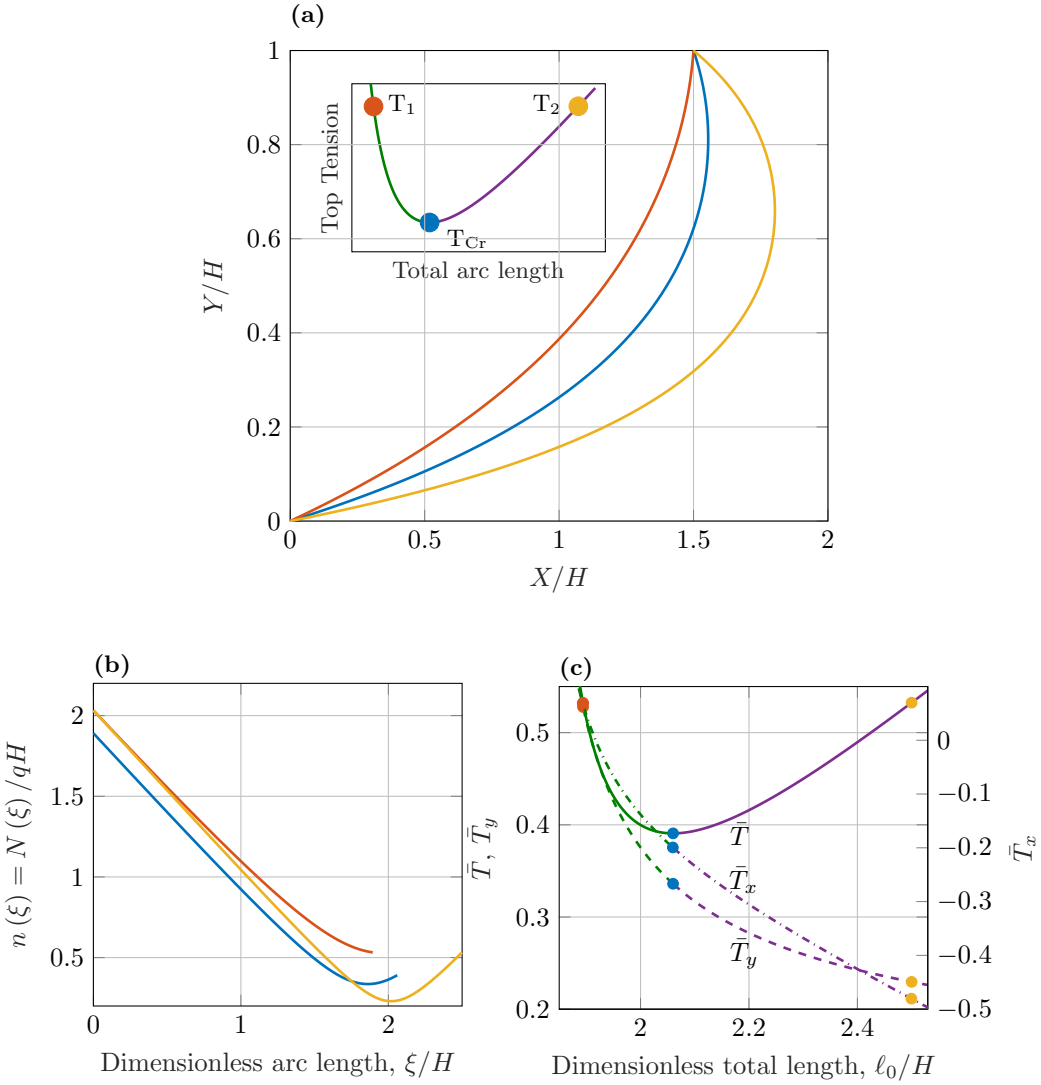

Fig. 4. Configurations of an inextensible riser subject to a constant horizontal force $\mathbf{F} = q\mathbf{E}_1$: (a) static equilibrium configurations with a critical top tension (blue line), one with a specified top tension and a shorter overall length ℓ_0 (red line), and one with the same specified top tension but with a longer overall length ℓ_0 (yellow line), (b) variation of the dimensionless tension n along the entire length of cable for the three static configurations show that the configurations are all in tension throughout their entire length, and (c) decomposition of the magnitude of the dimensionless top tension $\bar{T}$ into its horizontal $\bar{T}_x$ and vertical $\bar{T}_y$ components for a range of values of the overall length ℓ_0 shows that the behavior of $\bar{T}_x$ and $\bar{T}_y$ are not indicative of the magnitude $\bar{T}$. The dimensionless tensions are defined in Eqn. (3.10).

3.2. Application to a neutrally buoyant riser

We now consider the static configurations of a neutrally buoyant riser that were originally examined by Chucheepsakul and Wang (1997). For such a riser, the buoyancy

force balances gravity and the resultant force acting on the riser is in the horizontal direction:

$$\mathbf{F} = q\mathbf{E}_1. \tag{3.8}$$

Representative solutions to this problem for an inextensible string (each with a different value of ℓ_0) are shown in Fig. 4(a):

$$Y_H = H = 40.0\,\mathrm{m}, \qquad \frac{X_H}{H} = \frac{3}{2}, \qquad q = 10.0\,\mathrm{kN/m}, \tag{3.9}$$

where H is the depth of the water at $\mathcal{O}$. The tension in the string is non-dimensionalized using the parameter qH and the arc length parameter ξ of the string is non-dimensionalized using the parameter H:

$$n\left(\xi\right) = \frac{1}{qH}N\left(\xi\right), \qquad \bar{T} = \frac{1}{qH}T_{\mathrm{Top}}, \qquad \bar{T}_x = \frac{1}{qH}\mathbf{N}\left(\ell_0\right)\cdot\mathbf{E}_1, \qquad \bar{T}_y = \frac{1}{qH}\mathbf{N}\left(\ell_0\right)\cdot\mathbf{E}_2. \tag{3.10}$$

We have taken the liberty of defining the dimensionless horizontal and vertical components of the top tension.

As first astutely observed by Chucheepsakul and Wang (1997), if we parameterize the solutions to the boundary value problem using the top tension T_{Top}, then two possible solutions (each with a different ℓ_0 and a different value of $\alpha_1\left(\ell_0, t\right)$) are possible provided T_{Top} is greater than a critical value. These authors described this value as the critical top tension: T_{Cr}. If T_{Top} is lower than this value then no static configuration is possible. Their results are reproduced in Fig. 4(a). These authors state that, for a given value of T_{Top}, the configuration with the shorter length ℓ_0 is stable and the configuration with the longer length is unstable. The stability criterion they employ was further elaborated upon in a later work (see Chucheepsakul and Monprapussorn (2001)). It is important to note that their criterion is different both to the nonlinear stability criterion and the linear vibration analysis used in the present paper.

To examine if a static equilibrium is stable, we apply criterion SC-1 to the configurations shown in Fig. 4(a). The criterion simply involves checking if the tension N in the string is always positive. As shown in Fig. 4(b), N is always positive for each of the three configurations. We therefore conclude that all three configurations are in fact nonlinearly stable. Furthermore, we have examined all the configurations of the riser shown in the inset image in Fig. 4(a) and found that $N(\xi) > 0$ throughout the length of the cable. In conclusion, the static equilibria of the riser are all nonlinearly stable.

It is also interesting in this example to compare the horizontal and vertical components of the top tension for each of the configurations shown in the inset image in Fig. 4(a). As shown in Fig. 4(c) there is no correlation between the variation of T_{Top} and the variation of its vertical T_y and horizontal T_x components.

We next consider the case of an extensible cable which has a strain-energy function

$$\Psi = \rho_0 A\psi = \frac{EA}{2}\left(\mu - 1\right)^2. \tag{3.11}$$

For this strain-energy function

$$\rho_0 A\frac{\partial^2\psi}{\partial\mu^2} - \frac{\rho_0 A}{\mu}\frac{\partial\psi}{\partial\mu} = \frac{EA}{\mu} > 0. \tag{3.12}$$

The solutions for this model of the riser are qualitatively similar to those shown in Fig. 4 for the inextensible string model. In the interests of brevity, they are not reproduced here. Additionally, because the elastic string is also never slack, we can apply criterion SC-2 to the static configurations of the elastic string and conclude that they too are nonlinearly stable.

The string model for the catenary-type riser is arguably too simplistic. Not only does it ignore the effects of the fluid it also ignores bending and torsional modes of deformation. It is clearly of interest to see if these additional effects can destabilize the static configuration.

4. Dynamics of a riser modeled as a heavy cable using a rod theory

We now turn to modeling the catenary-type riser attached to a point $\mathcal{O}$ on the seabed and a hang-off point $\mathcal{H}$ on the sea surface using Kirchoff's rod theory. To help place our work in the context of other works by Chucheepsakul and Monprapussorn (2001) and Athisakul et al. (2014) we use the set of parameters are identical to those for Model 1 in Table 1. The rod resists bending and torsion and is extensible.

As anticipated, we find that the static configurations of the riser are qualitatively similar to those we found using a string model. Some of these configurations are shown in Figure 5(a). As found by Chucheepsakul and Monprapussorn (2001), if we classify the solutions using the top tension T_{Top} as a function of the undeformed arc length of the riser, then the curve shown in Figure 5(b) is found. The values of $\mathbf{N}(\ell_0)$ for the configurations labelled (1)–(7) in Figure 5(a) are presented in Table 2.

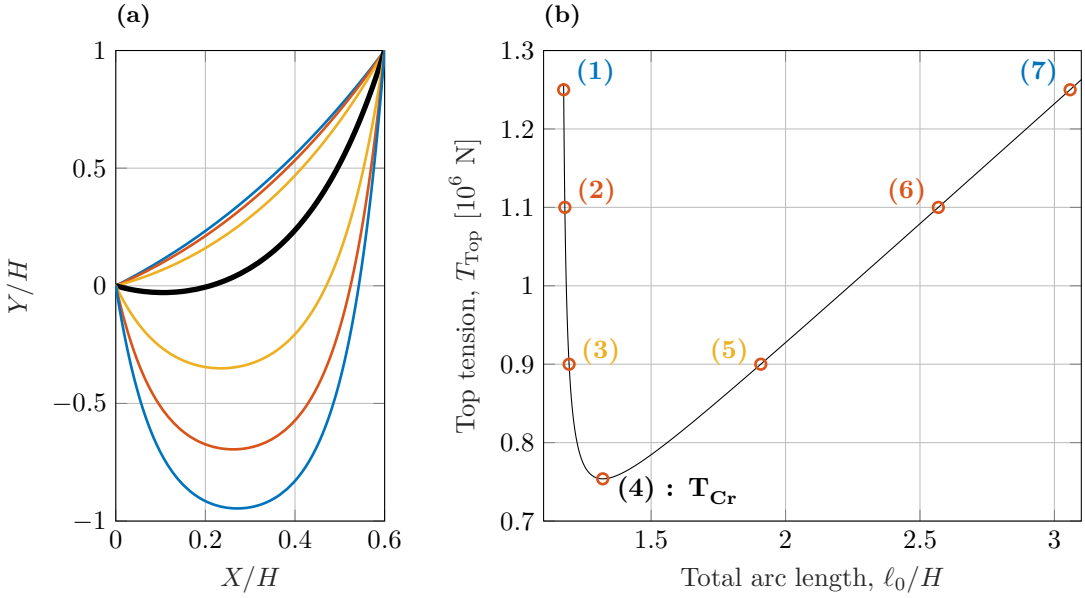

Fig. 5. (a) Static equilibrium configurations corresponding to distinct values of the top tension T_{Top}. (b) Variation of the top tension at the hang-off point $\mathcal{H}$ as a function of the overall length ℓ_0 of the undeformed rod. The riser is modeled as an extensible rod with the parameter values for Model 1 (cf. Table 1). The magnitudes and directions of the top tensions corresponding to the labels (1)–(7) are presented in Table 2.

Table 2. The magnitude T_{Top} and direction $\alpha_1\,(\ell_0, t)$ of the tension force $\mathbf{N}$ at the hang-off point $\mathcal{H}$ for the seven configurations for Model 1.

Number of Configuration	Tension Force $\mathbf{N}\,(\ell_0)$ at $\mathcal{H}$	
	Magnitude T_{Top} [10^4N]	Direction $\alpha_1\,(\ell_0, t)$ [rad]
(1)	1.25	1.1989
(2)	1.10	1.2242
(3)	0.90	1.2840
(4)*	0.75	1.4096
(5)	0.90	1.4942
(6)	1.10	1.5190
(7)	1.25	1.5289

* indicates the configuration which has the critical top tension.

The stability criterion used by Chucheepsakul and Wang (1997) for the string model of the riser has been extended to various types of marine structures from vertical risers and steel catenary risers to marine risers transporting fluid by Chucheepsakul and Monprapussorn (2001) and Athisakul et al. (2014). Using their stability criterion, out of two static configurations having the identical values of top tension applied at the hang-off

point, the one with the shorter arc length (e.g., the configurations (1), (2), and (3) shown in Fig. 5(a)) are considered to be stable while those with the longer arc length (e.g., the configurations (5), (6), and (7)) are considered to be unstable. Their use of $T_{\text{Top}}(\ell_0)$ as a stability criterion appears to motivated from works on the stability of columns and straight rods subject to constant vertical loads. However, in the riser, the force $\mathbf{N}(\ell_0)$ at the hang-off point also has a direction that must be considered in any stability criterion.

Table 3. The lowest four eigenvalues for each of the seven static equilibrium configurations shown in Fig. 5(a) for Model 1.

No. of Conf.	Complex eigenvalues [rad/s]							
	Mode 1		Mode 2		Mode 3		Mode 4	
	Re(λ)	Im(λ)	Re(λ)	Im(λ)	Re(λ)	Im(λ)	Re(λ)	Im(λ)
(1)	-0.0000	0.3507	-0.0000	0.7011	-0.0000	1.0515	-0.0000	1.4021
(2)	-0.0000	0.3174	-0.0000	0.6343	-0.0000	0.9513	-0.0000	1.2685
(3)	-0.0000	0.2628	-0.0000	0.5246	-0.0000	0.7864	-0.0000	1.0485
(4)*	-0.0000	0.1828	-0.0000	0.3611	-0.0000	0.5371	-0.0000	0.7140
(5)	-0.0000	0.1324	-0.0000	0.2429	-0.0000	0.3473	-0.0000	0.4639
(6)	-0.0000	0.1127	-0.0000	0.1917	-0.0000	0.2770	-0.0000	0.3729
(7)	-0.0000	0.1033	-0.0000	0.1682	-0.0000	0.2481	-0.0000	0.3324

* indicates the configuration which has the critical top tension.

4.1. Linear vibration analysis

To explore the stability of a configuration of the riser, we examine the linear vibrations of the riser about a static configuration. Prior to discussing our results, we note that we validated our numerical methods by comparing our results to those presented in the literature. Further details on the validation are discussed in Appendix B. For the static configurations labeled (1) to (7) in Fig. 5, we computed the real and imaginary parts of the eigenvalues for the first four out-of-plane(lateral) modes. The results are presented in Table 3. The mode shapes corresponding to the lowest four natural frequencies for configurations (2) and (6) that have identical values of top tension at the hang-off point are shown in Fig. 6 and 7, respectively. The lowest frequency modes for these configurations are lateral out-of-plane modes in Z-direction. The most important conclusion from our computation of eigenvalues is that configurations (1) through (7) are *all* linearly stable (i.e., all the eigenvalues are purely imaginary). This result is also in agreement with our earlier conclusions based on a string model for the catenary-type riser.

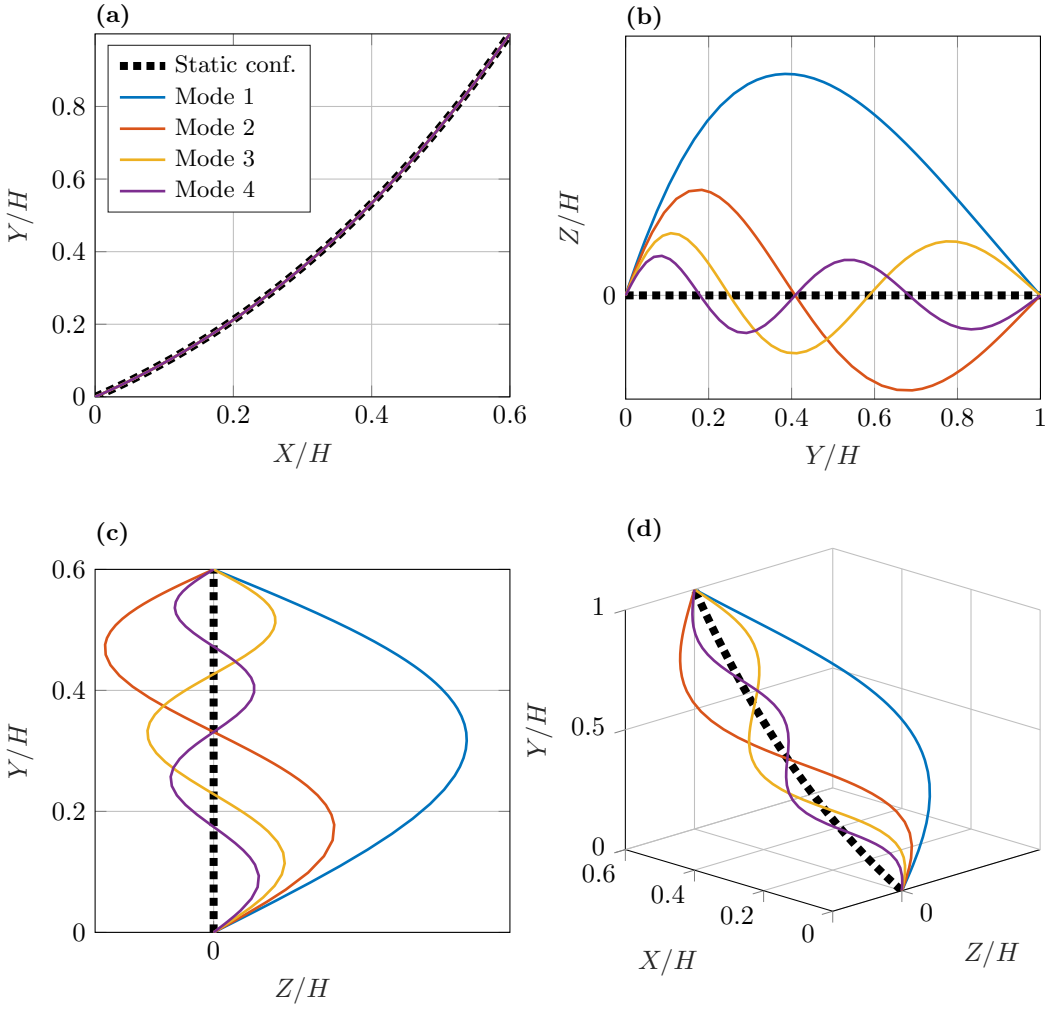

Fig. 6. Mode shapes of the first four modes for the static configuration (2) shown in Fig. 5(a): (a) on XY plane; (b) on YZ plane; (c) on ZX plane; and (d) in the three dimensional space. The modes in question are all lateral or out-of-plane modes.

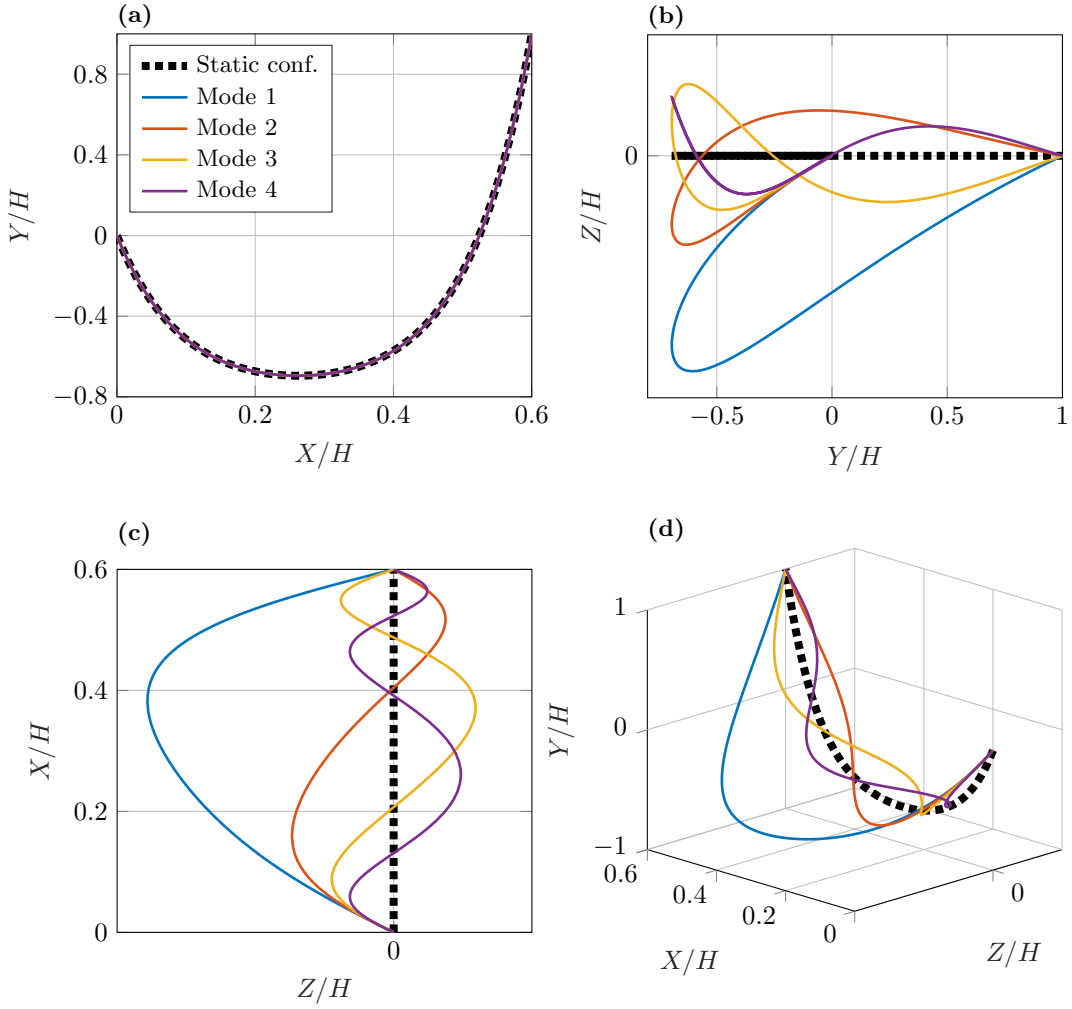

Fig. 7. Mode shapes of the first four modes for the static configuration (6) shown in Fig. 5(a): (a) on XY plane; (b) on YZ plane; (c) on ZX plane; and (d) in the three dimensional space. The modes in question are all lateral or out-of-plane modes.

4.2. Fluid-induced destabilization

The previous analysis of the catenary-type riser's static configuration and the concomitant linear stability ignored the effects of external fluid moving with a horizontal speed of V_F and a fluid that is being transported inside the riser at a constant speed V_i. Our next set of analyses take these effects into account. For the purpose of that, we use the parameter values for Model 3 given in Table. 1.[4] The same procedures introduced previously are conducted and a variety of static equilibrium configurations corresponding

[4]We note that Model 1 and Model 2 ignore the effects of fluid being transported internally by the riser.

to distinct value of arc length ℓ_0 are shown in 8(a), and the corresponding top tension as a function of the total arc length is displayed in Fig. 8(b). In the interest of brevity, we show the lowest four complex eigenvalues (C.5) and corresponding mode shapes (Fig. C.14 and C.15) for Model 3 in Appendix C. Similar to the previous results for Model 1, those results show that all of the static configurations for Model 3 are stable when either the external and internal fluid is not taken into account.

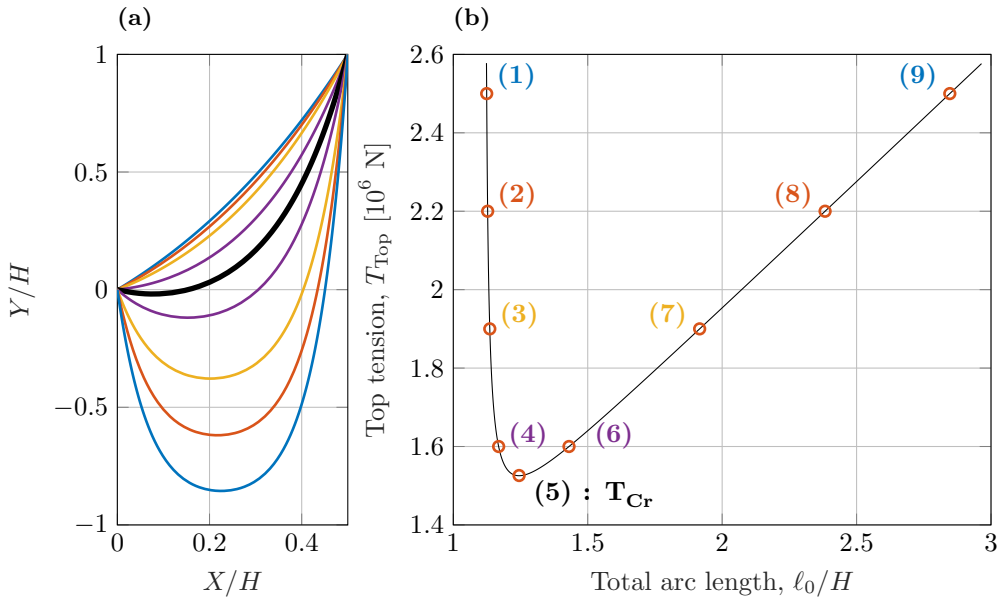

Fig. 8. (a) Static equilibrium configurations corresponding to distinct values of the top tension T_{Top}. (b) Variation of the top tension at the hang-off point $\mathcal{H}$ as a function of the overall length ℓ_0 of the undeformed rod. The riser is modeled as an extensible rod with the parameter values for Model 3 (cf. Table 1). The values and magnitudes of the top tensions and the lowest frequencies for the static configurations labeled (1)–(9) are presented in Table C.5.

4.2.1. The effects of a steady current

To examine the effects of a steady current with the constant value of speed in $\mathbf{E}_1$ direction, the current speed V_F is varied from 0 m/s to 2 m/s for the configurations labeled (1)-(9) in Fig. 8. As shown in Fig. 9, it is easy to observe the effect that the external current has on the static configuration. As expected, we also find that some of these static configurations with a longer length ℓ_0 are significantly effected by the external fluid flow while those with a shorter length are not. In addition, as shown in the inset images in Fig. 9, the current also effects the top tension. In particular, the value of the top tension applied to the longer configurations increases with increasing current speed, while the top tension in the shorter configurations does not change significantly.

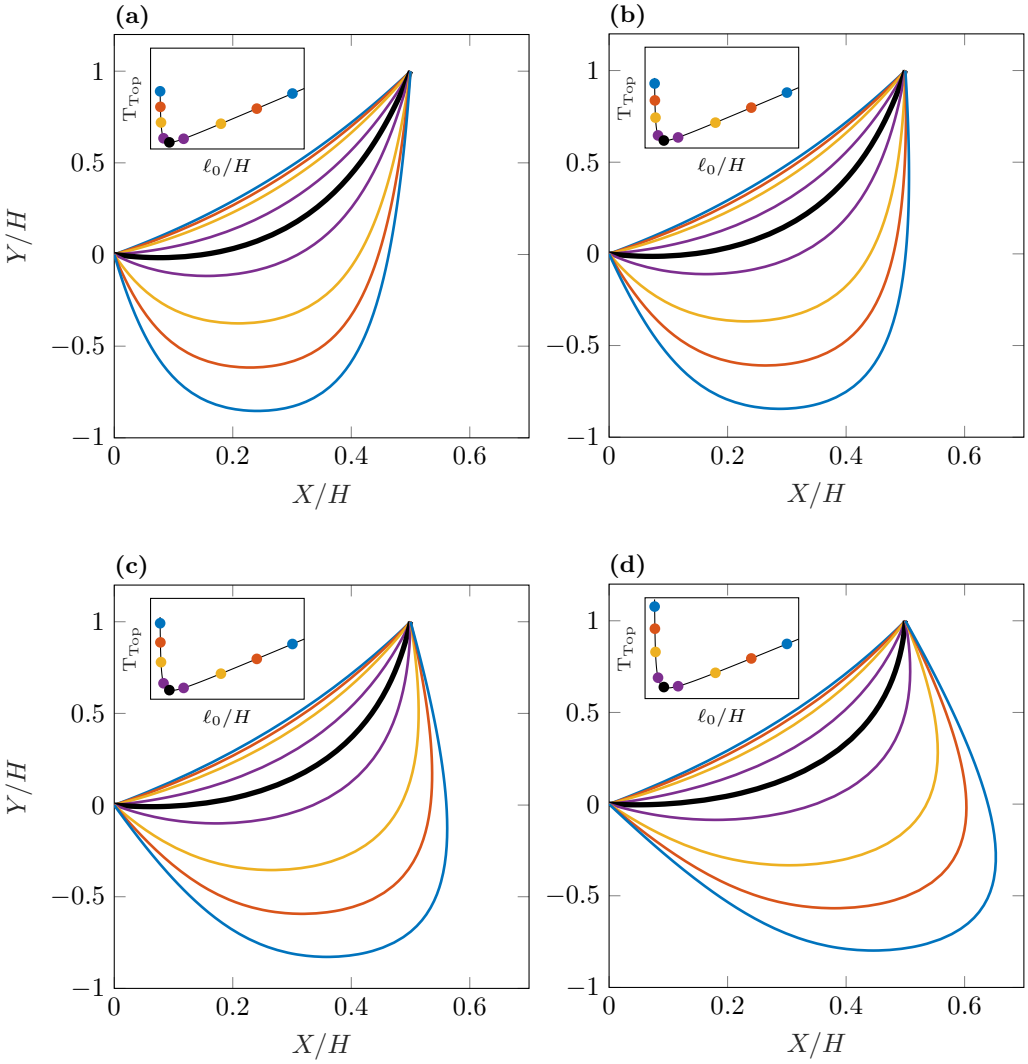

Fig. 9. Variation of the static equilibrium configurations and corresponding magnitude of top tension applied at the hang-off point $\mathcal{H}$ of a riser subject to the forces due to a steady current $V_F\mathbf{E}_1$: (a) 0.5, (b) 1.0, (c) 1.5, and (4) $2.0m/s$. Note that these figures show the effects of applying the external current on the static configurations shown in Fig. 8, where the steady current is assumed to be constant in $\mathbf{E}_1$ direction. The parameter values for the rod that is used to model the riser are described by Model 3 in Table 1.

Consider an arbitrary pair of two different static solutions, e.g., (3) and (7) in Fig. 8(a), which have the same magnitude of top tension. The variation of the lowest four eigenvalues for this pair of configurations as the current speed is varied from 0 to 2 m/s is shown in Fig. 10. It is seen that according to the increase of external current, both configurations remain linearly stable. Compared to the results for the shorter

configuration (3) shown in Fig. 10(a), the longer configuration (7) shows a remarkable change in natural frequencies with increase of current velocity (cf. Fig. 10(b)). Despite these differences between the two configurations, they are both stable when any value of current speed is applied without considering internal fluid inside the riser. The same tendency showing the effect of external current on the global behavior in terms of natural frequencies can be seen on the other pair of static configurations, e.g., (2) and (8), can be seen in Fig. C.16 in Appendix C. Similar to the lateral out-of-plane modes, the behavior of the flexural in-plane modes with increasing external steady current was also examined. We verified that the in-plane flexural modes decay and thus do not effect the stability of the static configuration.

4.2.2. The effects of transporting a fluid

Next, we examined the effect of internal fluid on the stability of the riser, for three static configurations: a short configuration (3) and a longer one (7) that have the identical magnitude of top tension when $V_i = 0$, and a configuration (5) whose top tension is the critical value. A constant internal fluid with speed V_i ranging from 0 to 100 m/s was applied. Before discussing the effect of internal flow on the natural frequencies, it is noted that in agreement with earlier results by Santillan et al. (2010), the internal fluid flow has little effect on the shape of the static configuration of the riser. As can be seen from Fig. 11, the internal fluid does effect the tension n_3 but $n_3 - \mu {v_i}^2$ is unchanged. Thus, the dimensionless tension in the string is increased by an amount $\mu {v_i}^2$.

The corresponding variation of the eigenvalues for the three configurations labeled (3), (5), and (7) in Fig. 8(a) are shown in Fig. 12.[5] As shown in Fig. 12(a), (c), and (e), and in contrast to the case where V_F alone was varied, the internal flow, V_i, slightly decreases the natural frequencies for all three configurations of interest. More significantly, as shown in Fig. 12(b), (d), and (f), the configurations (3) and (5) are linearly stable whereas configuration (7) destabilizes by a flutter instability (or Hopf bifurcation) once $V_i \neq 0$. In particular, the second and third modes become unstable. Typically, the internal fluid is transported at an average speed of 0 to 30 m/s. In order to emphasize that the stability characteristics does not change with increasing flow rate, we increased the speed of internal fluid up to 100 m/s to verify that the configurations maintained their stability characteristics.

We explored the stability of other few configurations in Fig. 9 and concluded that, for a given top tension, the configuration with the shorter length will remain stable even when the effects of internal fluid transport are considered. However, the configuration with the longer length will immediately lose stability once $V_i \neq 0$. Given a value of the top tension, we note that the tendency for the shorter configuration to be stable while the longer configuration is unstable is also observed for the rod Model 3 in Table 1 (cf. Fig. C.17 in Appendix C). The flutter instability of the configurations in Fig 8(a) discussed above is similar to the instability found in the classic problem of a vertical riser conveying fluid (and the closely related problem of a cantilevered pipe conveying fluid).[6] In contrast to the catenary-type riser, for the vertical riser (and the related problem of a cantilevered pipe conveying fluid), V_i must be larger than a non-zero critical value

[5]The corresponding mode shapes are shown in Figs. C.14 and C.15 in Appendix C.

[6]We refer the reader to Chatjigeorgiou (2010), Ghayesh et al. (2011), and Païdoussis (2014) for discussions of the extensive literature on these problems.

for the riser to become unstable. The precise value of the critical speed depends on the parameters such as flexural rigidity and the dimensions of the pipe. However, as discussed in Kuiper (2008), if the cantilevered pipe is considered to be of infinite length, then a flutter instability occurs when $V_i \neq 0$.

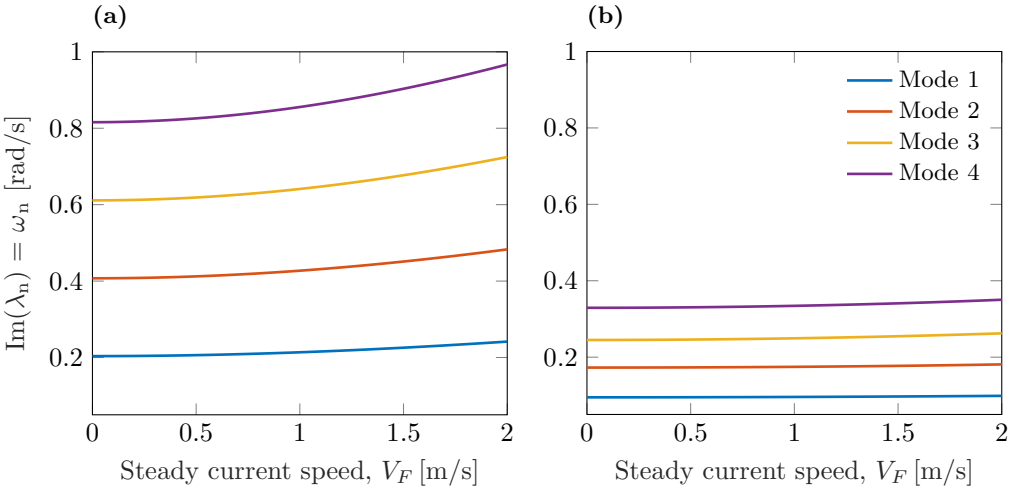

Fig. 10. Variation of the lowest four natural frequencies (i.e., imaginary part of the eigenvalues $\mathrm{Im}(\lambda_n) = \omega_n$) with increase in the steady current speed: (a) for the configuration (3) shown in Fig. 8(b), and (b) for the configuration (7) which has a longer arc length than (3) and is shown in Fig. 8(b). Note that the lowest four eigenvalues for both cases are almost purely imaginary ($Re(\lambda_n) = 0$), and hence both configuration are linearly stable.

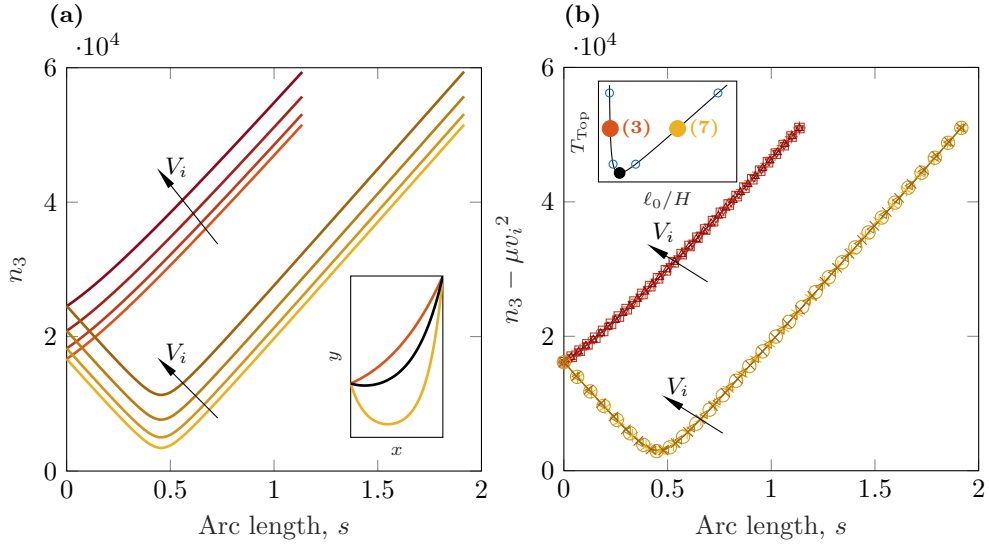

Fig. 11. Variation of (a) the tension force (internal force) n_3, and (b) the "effective" tension force $n_3 - \mu {v_i}^2$ with varying values of the internal fluid speed, V_i: 25, 50, 75, and 100 m/s. The red curves are for the shorter configuration (3) while the yellow curves pertain to the longer configuration (7) shown in Fig. 8(b). Both of these configurations have the same top tension.

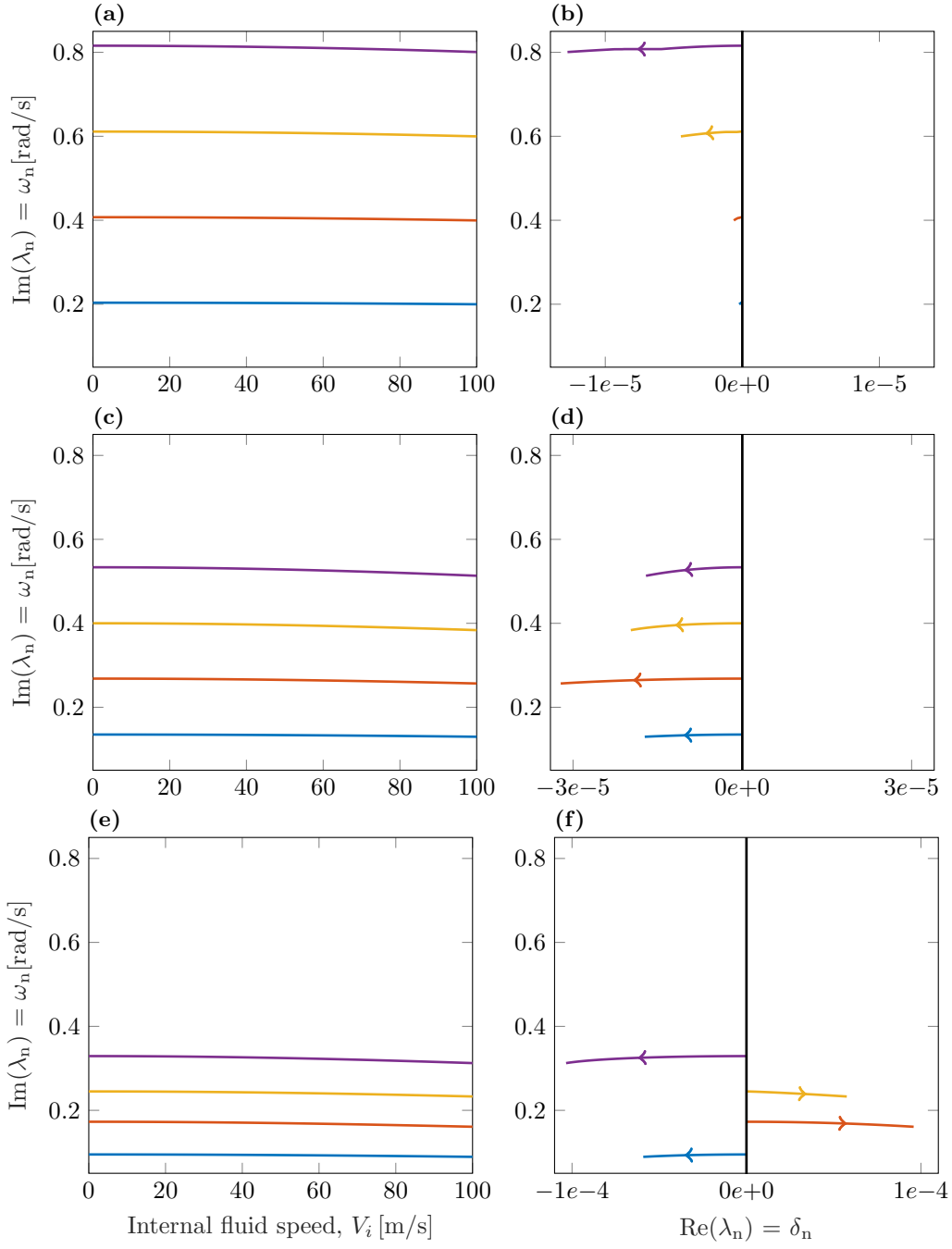

Fig. 12. Behavior of the first four vibration modes as the speed of internal fluid (V_i) is varied for the equilibrium configurations (3), (5), and (7) shown in Fig. 8(a). Two of these configurations, (3) and (7), have the same top tension applied at the hang-off point and (5) is the configuration with the critical value of top tension: (a), (c), and (e): show the variation of natural frequencies for the static configurations labeled (3), (5), and (7), respectively; and (b), (d), and (f): show the behavior of the lowest four modes for the static configurations labeled (3), (5), and (7), respectively, on the complex plane as the internal fluid speed V_i is varied. The arrows indicate the direction of increasing flow rate V_i.

5. Conclusions

This paper has presented an investigation of the stability of catenary-type risers in deep waters. The simplest models of these risers assume that they can be modeled as a perfectly flexible string pinned at both ends and acted upon by a conservative force field. We find that the static configurations predicted by these models are always nonlinearly stable. When more sophisticated rod-based models that include the effects of internal fluid transport in the riser are analyzed, we find that certain static configurations of the riser can be destabilized in a flutter instability. These results complement earlier works by Chucheepsakul et al. who classified risers using a concept known as the top tension T_{Top}. They found, for a given T_{Top}, two configurations were possible with distinct overall lengths. The configuration with the shorter (longer) length was deemed to be stable (unstable) using a different stability criterion than the ones we have chosen to use. Based on the stability criterion and modeling assumptions we have employed, we also find that the configuration with the shorter length is stable. However, for the configuration with the longer length to destabilize we have shown that it must convey fluid. The onset of instability is immediate once the internal fluid flow $V_i \neq 0$.

References

Antman, S. S., 2005. Nonlinear Problems of Elasticity, 2nd Edition. Vol. 107 of Applied Mathematical Sciences. Springer-Verlag, New York.
URL http://dx.doi.org/10.1007/0-387-27649-1

Atanackovic, T., 1997. Stability Theory of Elastic Rods. World Scientific.
URL https://doi.org/10.1142/9789812819673

Athisakul, C., Klaycham, K., Chucheepsakul, S., 2014. Critical top tension for static equilibrium configuration of a steel catenary riser. China Ocean Engineering 28 (6), 829–842.
URL https://doi.org/10.1007/s13344-014-0064-x

Bai, Y., Bai, Q., 2005. Subsea Pipelines and Risers. Elsevier, Amsterdam.
URL https://dx.doi.org/10.1016/b978-0-08-044566-3.x5000-3

Chatjigeorgiou, I. K., 2008. A finite differences formulation for the linear and nonlinear dynamics of 2D catenary risers. Ocean Engineering 35 (7), 616–636.
URL http://doi.org/10.1016/j.oceaneng.2008.01.006

Chatjigeorgiou, I. K., 2010. On the effect of internal flow on vibrating catenary risers in three dimensions. Engineering Structures 32 (10), 3313–3329.
URL https://doi.org/10.1016/j.engstruct.2010.07.004

Chucheepsakul, S., Monprapussorn, T., 2001. Nonlinear buckling of marine elastica pipes transporting fluid. International Journal of Structural Stability and Dynamics 1 (03), 333–365.
URL https://doi.org/10.1142/S0219455401000263

Chucheepsakul, S., Monprapussorn, T., Huang, T., 2003. Large strain formulations of extensible flexible marine pipes transporting fluid. Journal of Fluids and Structures 17 (2), 185 – 224.
URL https://doi.org/10.1016/S0889-9746(02)00116-0

Chucheepsakul, S., Srinil, N., 2002. Free vibrations of three-dimensional extensible marine cables with specified top tension via a variational method. Ocean Engineering 29 (9), 1067–1096.
URL https://doi.org/10.1016/S0029-8018(01)00064-6

Chucheepsakul, S., Wang, C. M., 1997. Mechanics of neutrally bouyant cables. Mechanics Research Communications 24 (6), 603–607.
URL https://doi.org/10.1016/S0093-6413(97)00077-3

Doaré, O., 2019. Dissipation induced instabilities of structures coupled to a flow. In: Bigoni, D., Kirillov, O. (Eds.), Dynamic Stability and Bifurcation in Nonconservative Mechanics. CISM International Centre for Mechanical Sciences (Courses and Lectures). Vol. 586. Springer-Verlag, Berlin, Heidelberg, pp. 63–102.
URL https://doi.org/10.1007/978-3-319-93722-9_2

Ertas, A., Kozik, T. J., 1987. A review of current approaches to riser modeling. Journal of Energy Resources Technology 109 (3), 155–160.
URL https://doi.org/10.1115/1.3231341

Garrett, D. L., 1982. Dynamic analysis of slender rods. Journal of Energy Resources Technology 104 (4), 302–306.
URL https://doi.org/10.1115/1.3230419

Ghayesh, M. H., Païdoussis, M. P., Modarres-Sadeghi, Y., 2011. Three-dimensional dynamics of a fluid-conveying cantilevered pipe fitted with an additional spring-support and an end-mass. Journal of Sound and Vibration 330 (12), 2869–2899.
URL https://doi.org/10.1016/j.jsv.2010.12.023

Kuiper, G. L., 2008. Stability of offshore risers conveying fluid. Ph.D. thesis, TU Delft, Delft University of Technology.

Love, A., 1927. A Treatise on the Mathematical Theory of Elasticity, 4th Edition. Cambridge University Press, Cambridge.

Meng, D., Chen, L., 2012. Nonlinear free vibrations and vortex-induced vibrations of fluid-conveying steel catenary riser. Applied Ocean Research 34, 52–67.
URL https://doi.org/10.1016/j.apor.2011.10.002

Monprapussorn, T., Athisakul, C., Chucheepsakul, S., 2006. Nonlinear vibrations of an extensible flexible marine riser carrying a pulsatile flow. Journal of Applied Mechanics 74 (4), 754–769.
URL https://doi.org/10.1115/1.2711226

Morison, J., Johnson, J., Schaaf, S., 1950. The force exerted by surface waves on piles. Journal of Petroleum Technology 2 (5), 149–154.
URL https://doi.org/10.2118/950149-g

Neto, A. G., Martins, C. A., 2013. Structural stability of flexible lines in catenary configuration under

torsion. Marine Structures 34, 16–40.
URL https://doi.org/10.1016/j.marstruc.2013.07.002
Neukirch, S., Frelat, J., Goriely, A., Maurini, C., 2012. Vibrations of post-buckled rods: the singular inextensible limit. Journal of Sound and Vibration 331 (3), 704–720.
Nordgren, R. P., 1974. On computation of the motion of elastic rods. Journal of Applied Mechanics 41 (2), 777–780.
URL https://doi.org/10.1115/1.3423387
O'Reilly, O. M., 1996. Steady motions of a drawn cable. Journal of Applied Mechanics 63 (1), 180–189.
URL https://doi.org/10.1115/1.2787196
O'Reilly, O. M., 2017. Modeling Nonlinear Problems in the Mechanics of Strings and Rods. Springer-Verlag, New York.
URL http://dx.doi.org/10.1007/978-3-319-50598-5
Païdoussis, M., 2014. Fluid-Structure Interactions, Slender Structures and Axial Flow. Vol. 1. Academic Press, San Diego, California, USA.
URL https://doi.org/10.1016/c2011-0-08057-2
Patel, M., Seyed, F., 1995. Review of flexible riser modelling and analysis techniques. Engineering Structures 17 (4), 293–304.
URL http://dx.doi.org/10.1016/0141-0296(95)00027-5
Rombado, G., Yue, B., Rueda, C., 2012. Steel catenary jumper for single hybrid riser in deepwater applications. In: Offshore Technology Conference, 30 April-3 May, Houston, Texas, USA. Offshore Technology Conference, pp. 1–17.
URL https://doi.org/10.4043/23704-MS
Ruan, W., Bai, Y., Cheng, P., 2014. Static analysis of deepwater lazy-wave umbilical on elastic seabed. Ocean Engineering 91, 73–83.
URL https://dx.doi.org/10.1016/j.oceaneng.2014.08.017
Santillan, S. T., Virgin, L. N., Plaut, R. H., 2010. Static and dynamic behavior of highly deformed risers and pipelines. Journal of Offshore Mechanics and Arctic Engineering 132 (2), 021401.
URL http://dx.doi.org/10.1115/1.4000555
Shampine, L. F., Gradwell, I., Thompson, S., 2003. Solving ODEs with MATLAB. Cambridge University Press, Cambridge.
URL http://dx.doi.org/10.1017/cbo9780511615542
Wang, J., Duan, M., He, T., Jing, C., 2014. Numerical solutions for nonlinear large deformation behaviour of deepwater steel lazy-wave riser. Ships and Offshore Structures 9 (6), 655–668.
URL http://dx.doi.org/10.1080/17445302.2013.868622
Wasserstrom, E., 1973. Numerical solutions by the continuation method. SIAM Review 15 (1), 89–119.
URL https://doi.org/10.1137/1015003

Appendix A. Scaling of the equations

Non-dimensionalization of the equations of motion are performed with length scaled using H, force using EI/H^2, moments using EI/H, and time using $H^2/\sqrt{\rho_0 A/(EI)}$. For the position vectors and arc-length coordinates, we employ the depth of the water at $\mathcal{O}$ relative to the hang-off point $\mathcal{H}$ to non-dimensionalize length variables:

$$\mathbf{r} = \frac{\mathbf{R}}{H}, \qquad x = \frac{X}{H}, \qquad y = \frac{Y}{H}, \qquad s = \frac{\xi}{H}, \tag{A.1}$$

We also choose the following dimensionless parameterizations of time, frequency, and fluid velocity,

$$\tau = \frac{t}{H^2}\sqrt{\frac{EI}{\rho_0 A}}, \qquad \Omega = \omega H^2\sqrt{\frac{\rho_0 A}{EI}}, \qquad v_i = V_i H\sqrt{\frac{\rho_i A_i}{EI}}, \tag{A.2}$$

and strains

$$\bar{\nu}_1 = \nu_1 H, \qquad \bar{\nu}_2 = \nu_2 H, \qquad \bar{\nu}_3 = \nu_3 H. \tag{A.3}$$

The external forces such as gravity, buoyancy, and drag force are scaled as follows:

$$w = \frac{\rho_o A g H^3}{EI}, \qquad b = \frac{\rho_f A_o g H^3}{EI}, \qquad f = \frac{0.5 \rho_f D \left\| \mathbf{v}_r \right\|^2 H^3}{EI}, \tag{A.4}$$

and the dimensionless slenderness parameter η, ratio of mass of pipe to internal flow β, and ratio of torsional to bending stiffness γ are defined as follows:

$$\eta = \frac{AL^2}{I}, \qquad \beta = \frac{\rho_i A_i}{\rho_0 A}, \qquad \gamma = \frac{\mathcal{D}}{EI}. \tag{A.5}$$

For the internal forces and moments, we employ the following non-dimensionalizations with help of (A.3) and γ:

$$\begin{aligned} \mathbf{n} &= \frac{\mathbf{N} H^2}{EI} = \frac{N_1 H^2}{EI}\mathbf{d}_1 + \frac{N_2 H^2}{EI}\mathbf{d}_2 + \frac{N_3 H^2}{EI}\mathbf{d}_3 = n_1 \mathbf{d}_1 + n_2 \mathbf{d}_2 + n_3 \mathbf{d}_3, \\ \mathbf{m} &= \frac{\mathbf{M} H}{EI} = \frac{EI \nu_1 H}{EI}\mathbf{d}_1 + \frac{EI \nu_2 H}{EI}\mathbf{d}_2 + \frac{D \nu_3 H}{EI}\mathbf{d}_3 = \bar{\nu}_1 \mathbf{d}_1 + \bar{\nu}_2 \mathbf{d}_2 + \gamma \bar{\nu}_3 \mathbf{d}_3. \end{aligned} \tag{A.6}$$

For the extensible rod, by inverting the constitutive relation $EA(\mu - 1) = N_3$, the stretch μ can be expressed as a combination of dimensionless variables:

$$\mu = 1 + \eta \, n_3. \tag{A.7}$$

We use this substitution when solving (2.18) for extensible rods and strings.

Appendix B. Validations of Static and Free-Vibration Analyses

For the purpose of validating both the accuracy of the set of governing equations (2.18) and the numerical method used to solve the boundary-value problem, we compared our predicted static configurations with those from Chucheepsakul and Srinil (2002) who modeled the riser as an extensible rod and Santillan et al. (2010) who used an inextensible rod for the same purpose (cf. Model 1 and Model 2 in Table 1). As can be seen from Fig. B.13, our static results are in good agreement for both types of riser. In addition to the static equilibrium configuration, other physical quantities such as internal force, moment distribution, and curvatures also compared favorably.

To validate our numerical methods used to compute the mode shapes, frequencies, and damping of the vibrations of a catenary-type riser that is modeled using a rod theory, we again compared our results to published results for two set of parameter values. To compute the free-vibration response of the riser, the system of linear amplitude equations (2.26) with the pinned boundary conditions specified at both ends of the riser are solved using the methods discussed in Section 2.4 and 2.5. As shown in Table B.4, the first set of natural frequencies obtained by solving the linear equations are in excellent agreement with the results in Chucheepsakul and Srinil (2002), Meng and Chen (2012), and Santillan et al. (2010).

We have also validated our numerical methods by reproducing the stability and instability results for a vertical and horizontal riser conveying fluid that is discussed by Monprapussorn et al. (2006) and Païdoussis (2014).

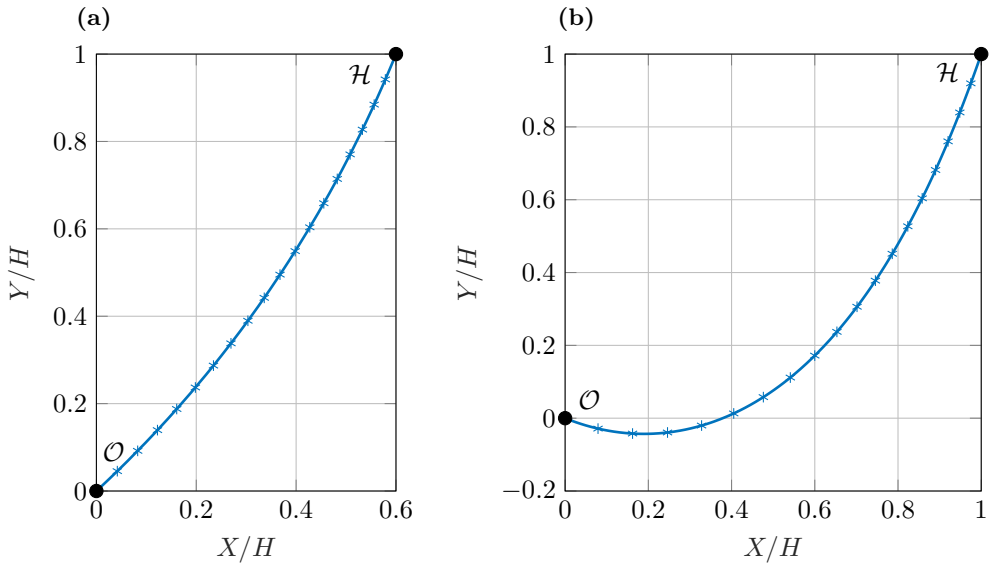

Fig. B.13. The static equilibrium configurations for catenary-type risers suspended from points $\mathcal{O}$ and $\mathcal{H}$ obtained using (2.18) and the solutions marked with a x obtained using a finite element method by Chucheepsakul and Srinil (2002) and a finite difference scheme and a shooting method Santillan et al. (2010), respectively. (a) The predicted static configuration when an extensible rod with a prescribed top tension ($25kN$) at the hang-off point $\mathcal{H}$ compared to the results (labeled x) of Chucheepsakul and Srinil (2002). (b) The predicted static configuration based on an inextensible riser compared to the results (labeled x) by Santillan et al. (2010).

Table B.4. The comparison of natural frequencies [rad/s] of catenary-type risers with previous works.

Unit	Model 1			Model 2	
[rad/s]	Current method	Chucheepsakul[a]	Meng[b]	Current method	Santillan[c]
Mode 1	0.5452	0.546	0.5491	0.2796	0.2790
Mode 2	1.0900	1.090	1.0992	0.4774	-
Mode 3	1.6350		-	0.6710	-
Mode 4	2.1800		-	0.8527	-

[a] Chucheepsakul and Srinil (2002).
[b] Meng and Chen (2012).
[c] Santillan et al. (2010).

Appendix C. Analysis of the Results for a Catenary-type Riser Modeled Using the Parameter Values for Model 3

The remarkable differences between Model 1 and Model 3 can be traced to modeling the transport of internal fluid. In particular, the results obtained from Model 3 whose parameter values shown in Table 1 represent the static and dynamic characteristics of the riser transporting a fluid. For example, Table C.5, Fig. C.14, and Fig. C.15 show that all the configurations labeled (1) to (9) shown in Fig. 8a and Table C.5 have purely imaginary eigenvalues and, thus, all the configurations are stable up to the first four modes. Providing that external and internal fluid effects are considered for the configurations labeled (2) and (8) shown in Fig. C.16 and Fig. C.17, we can see the same tendency concerning the effects of external and internal fluid on the riser behavior shown in Fig. 10 and Fig. 12 for the configurations labeled (3) and (7).

Table C.5. The lowest four eigenvalues for the static equilibrium configurations for Model 3 shown in Fig. 8.

No. of Conf.	Top Tension T_{Top} $[kN]$	Top Angle α_1 (ℓ_0) [rad]	Mode 1 [rad/s]	Mode 2 [rad/s]	Mode 3 [rad/s]	Mode 4 [rad/s]
(1)	2500	1.2536	0.2582	0.5165	0.7751	1.0341
(2)	2200	1.2783	0.2332	0.4665	0.7001	0.9342
(3)	1900	1.3149	0.2036	0.4072	0.6112	0.8158
(4)	1600	1.3834	0.1617	0.3232	0.4847	0.6472
(5)*	1525	1.4373	0.1350	0.2682	0.4001	0.5335
(6)	1600	1.4794	0.1146	0.2228	0.3258	0.4325
(7)	1900	1.5136	0.0949	0.1728	0.2450	0.3292
(8)	2200	1.5274	0.0848	0.1456	0.2085	0.2820
(9)	2560	1.5357	0.0777	0.1274	0.1864	0.2512

* Indicates the configuration which has the critical top tension.

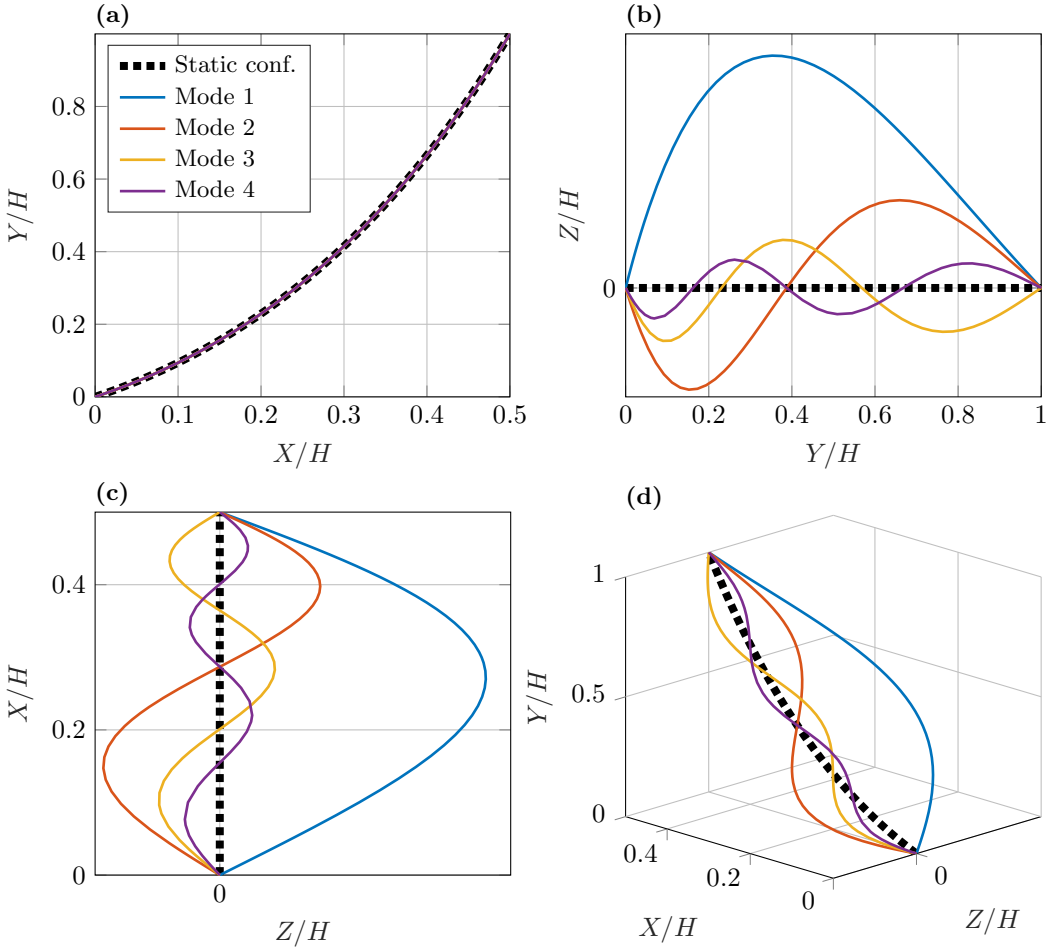

Fig. C.14. Mode shapes of the lowest four mode for the static configuration labeled (3) in Fig. 8: (a) on XY plane; (b) on YZ plane; (c) on ZX plane; and (d) in three-dimensional space

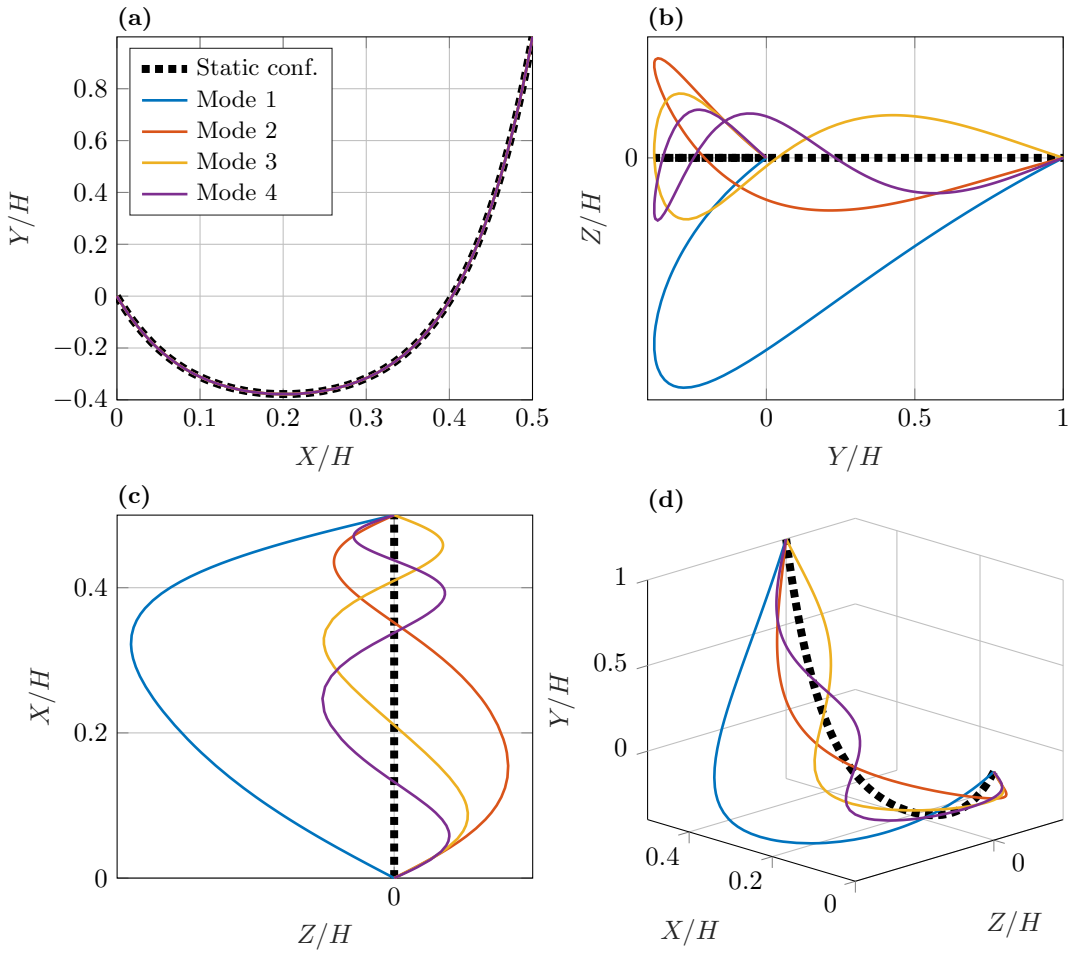

Fig. C.15. Mode shapes of the first four modes for the static configuration labeled (7) in Fig. 8: (a) on XY plane; (b) on YZ plane; (c) on ZX plane; and (d) in three-dimensional space

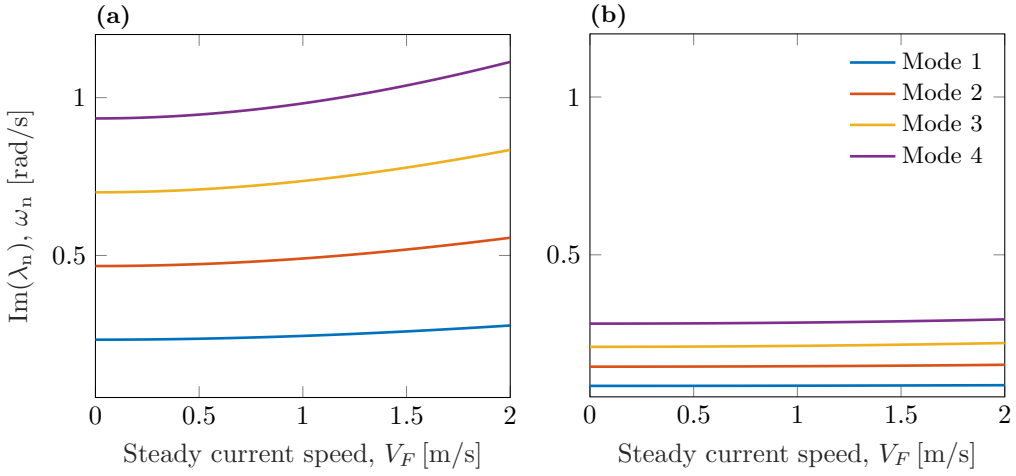

Fig. C.16. Variation of the first four natural frequencies (i.e., imaginary part of eigenvalues $\mathrm{Im}(\lambda_n) = \omega_n$) for various values of the steady current speed: (a) for the configuration labeled (2) in Fig. 8, and (b) for the configuration labeled (8) in Fig. 8. The configuration labeled (8) has a longer arc length than the configuration labeled (2). Note that the lowest four eigenvalues for both cases are nearly pure imaginary value ($Re(\lambda_n) = 0$), and consequently both configurations are linearly stable.

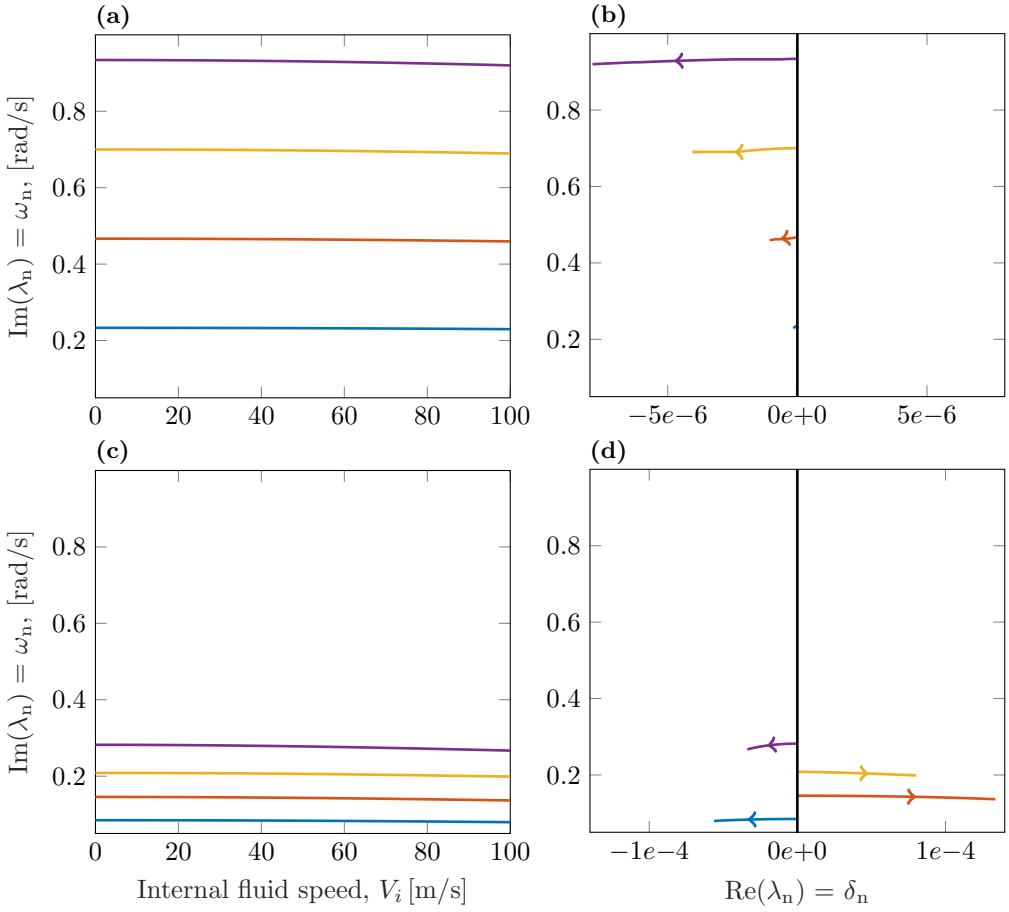

Fig. C.17. Behavior of the first four vibration modes as functions of the speed of internal fluid (V_i) for the static configurations labeled (2) and (8) in Fig. 8. This pair of equilibrium configurations have the same top tension applied at the hang-off point. (a) and (c): Variation of the natural frequencies for (2) and (8), respectively, and (b) and (d): behavior of the lowest four modes on the complex plane for (2) and (8), respectively, as the internal fluid speed V_i is varied. The arrows indicate the direction of increasing flow rate V_i. It should be noted that the configuration labeled (8) is linearly unstable when $V_i \neq 0$ while the other configuration (2) is linearly stable.